TKK Dissertations 120
Espoo 2008

OPTICAL AND ELECTRICAL INTERACTIONS IN SELF-ASSEMBLED METAL NANOPARTICLE SUPERSTRUCTURES

Doctoral Dissertation

Päivi Ahonen

Helsinki University of Technology
Faculty of Chemistry and Materials Sciences
Department of Chemistry

TKK Dissertations 120
Espoo 2008

OPTICAL AND ELECTRICAL INTERACTIONS IN SELF-ASSEMBLED METAL NANOPARTICLE SUPERSTRUCTURES

Doctoral Dissertation

Päivi Ahonen

Dissertation for the degree of Doctor of Science in Technology to be presented with due permission of the Faculty of Chemistry and Materials Sciences for public examination and debate in Auditorium KE2 (Komppa Auditorium) at Helsinki University of Technology (Espoo, Finland) on the 23rd of May, 2008, at 12 noon.

Helsinki University of Technology
Faculty of Chemistry and Materials Sciences
Department of Chemistry

Teknillinen korkeakoulu
Kemian ja materiaalitieteiden tiedekunta
Kemian laitos

Distribution:
Helsinki University of Technology
Faculty of Chemistry and Materials Sciences
Department of Chemistry
P.O. Box 6100
FI - 02015 TKK
FINLAND
URL: http://www.tkk.fi/Units/PhysicalChemistry/
Tel. +358-9-451 2572
Fax +358-9-451 2580
E-mail: Paivi.Ahonen@tkk.fi

ISBN 978-951-22-9361-2
ISBN 978-951-22-9362-9 (PDF)
ISSN 1795-2239
ISSN 1795-4584 (PDF)
URL: http://lib.tkk.fi/Diss/2008/isbn9789512293629/

TKK-DISS-2467

Multiprint Oy
Espoo 2008

ABSTRACT OF DOCTORAL DISSERTATION	HELSINKI UNIVERSITY OF TECHNOLOGY P. O. BOX 1000, FI-02015 TKK http://www.tkk.fi

Author Päivi Ahonen

Name of the dissertation

Optical and Electrical Interactions in Self-Assembled Metal Nanoparticle Superstructures

Manuscript submitted 12.2.2008	Manuscript revised
Date of the defence 23.5.2008	
☐ Monograph	☒ Article dissertation (summary + original articles)

Faculty	Faculty of Chemistry and Materials Science
Department	Department of Chemistry
Field of research	Physical Chemistry
Opponent(s)	Professor Jens Ulstrup
Supervisor (Instructor)	Professor Kyösti Kontturi

Abstract

Self-assembly of molecules and supramolecules is one of the fundamental phenomena in chemistry, physics, biology and material science. For example biological systems, like lipid bilayers of cell membranes and tertiary protein structures are formed by spontaneous self-assembly. Conformation and properties of these assemblies can be affected by changing the local environment of the structures. In the case of biological molecules, such an example would be protonation or deprotonation by changes in pH. When changing the conformation, one often changes the collective properties of the molecular assemblies.

In this thesis, the formation of functional nanoscale devices is approached from the self-assembly of molecules and metallic monolayer capped nanoparticles into superstructures consisting of numerous nanoparticles. Stabilisation of the individual nanosized particles is based on bonding between noble metals and thiol ligands. The desired chemical characteristics and functionality of the nanoparticles is achieved by choosing the capping ligand layer and thus, directing the interactions between the nanoparticles.

Both formation and functionality of the superstructures are studied in this thesis. Syntheses of silver and gold nanoparticles capped with different ligands are included. Both the individual nanoparticles and the colloidal superstructures formed by them were characterised by transmission electron microscopy (TEM), dynamic light scattering (DLS), zeta-potential measurements and UV-vis spectroscopy. Characterisation of the electrical properties of the self-assembled structures were carried out by scanning electrochemical microscopy (SECM).

The thesis is divided in three parts, considering first the formation of colloidal nanoparticle superstructures in solution, then a photoresponsive switching nanoparticle structure and finally electron transport processes in nanoscale films. In the first part, formation of nanoparticle aggregates via chemical and electrostatic interactions are studied. The second part consists of assembly and characterisation of a nanoswitch built from nanoparticles and photoisomerisable azobenzene molecules. In the last section of the thesis, electron transport processes in two self-assembled nanoscale films are studied with SECM. The first system is a molecular self-assembled monolayer and the second a film consisting of gold nanoparticles.

Keywords Nanoparticles, self-assembled monolayers, SECM, molecular switches

ISBN (printed)	978-951-22-9361-2	ISSN (printed)	1795-2239
ISBN (pdf)	978-951-22-9362-9	ISSN (pdf)	1795-4584
Language	English	Number of pages	68 p. + 44 p.
Publisher	Department of Chemistry		
Print distribution	Department of Chemistry		

☒ The dissertation can be read at http://lib.tkk.fi/Diss/2008/isbn9789512293629/

VÄITÖSKIRJAN TIIVISTELMÄ	TEKNILLINEN KORKEAKOULU PL 1000, 02015 TKK http://www.tkk.fi

Tekijä Päivi Ahonen

Väitöskirjan nimi

Optiset ja sähköiset vuorovaikutukset itsejärjestäytyneissä nanopartikkelirakenteissa

Käsikirjoituksen päivämäärä 12.2.2008	Korjatun käsikirjoituksen päivämäärä
Väitöstilaisuuden ajankohta 23.5.2008	
☐ Monografia	☒ Yhdistelmäväitöskirja (yhteenveto + erillisartikkelit)

Tiedekunta	Kemian ja materiaalitieteiden tiedekunta
Laitos	Kemian laitos
Tutkimusala	Fysikaalinen kemia
Vastaväittäjä(t)	Professori Jens Ulstrup
Työn valvoja (Työn ohjaaja)	Professori Kyösti Kontturi

Tiivistelmä

Molekyylien itsejärjestäytyminen eli molekyylirakenteiden spontaani muodostuminen on hyvin keskeinen luonnontieteilijöitä kiinnostava ilmiö. Itsejärjestymistä esiintyy muun muassa biologisissa systeemeissä, esimerkkeinä voidaan pitää vaikkapa lipidien asettumista levymäiseksi kaksikerrosrakenteeksi solukalvon muodostuessa sekä proteiinien tertiäärisiä rakenteita. Muuttamalla tällaisten molekyylirakenteiden ympäristöä, biologisissa systeemeissä esimerkiksi pH:ta, voidaan molekyylien konformaatiota eli avaruusrakennetta muuttaa. Konformaationmuutokset johtavat tyypillisesti myös molekyylirakenteen kollektiivisten ominaisuuksien muuttumiseen.

Tässä väitöskirjassa tutkitaan toiminnallisten nanomittakaavan rakenteiden muodostamista itsejärjestäytymisen avulla. Tutkitut systeemit ovat metallisista, orgaanisella ligandikerroksella stabiloiduista nanopartikkeleista muodostuneita rakenteita. Ligandikerroksen kemiallinen luonne vaikuttaa rakenteiden muodostumiseen ja toiminnallisuuteen ja se voidaan valita sovellukseen riippuen tilanteeseen sopivaksi. Tutkimuksessa käsitellään sekä yo. rakenteiden muodostumista että niiden toiminnallisia ominaisuuksia.

Menetelminä itsejärjestäytyneiden yksikerrosten sekä nanopartikkelisysteemien sähköisten ominaisuuksien tutkimisessa käytettiin sähkökemiallista pyyhkäisymikroskopiaa (SECM). Optisten ominaisuuksien tutkimisessa käytettiin spektrofotometriaa sekä valonsirontamittauksia (DLS). Sekä yksittäisten nanopartikkelien että niistä muodostuneiden rakenteiden muodosta ja koosta saatiin tietoa transmissioelektronimikroskopian (TEM) ja valonsironnan avulla.

Väitöskirjan ensimmäinen osa käsittelee kolloidisten nanopartikkelirakenteiden muodostumista, kun nanopartikkelien välillä on kemiallisia tai sähköstaattisia vuorovaikutuksia. Yhteenvedon toisessa osassa keskitytään optiseen nanokytkimeen, joka on muodostettu sitomalla nanopartikkeleita toisiinsa fotoisomeroituvan atsobentseenijohdannaisen avulla. Isomeroitumisreaktiossa partikkeleja sitovan molekyylin avaruusrakenne muuttuu, jolloin myös partikkelien välinen etäisyys muuttuu. Väitöskirjan kolmannessa osassa tutkitaan elektroninsiirtoprosesseja kahdessa erityyppisessä nanorakenteessa; atsobentseenijohdannaisen muodostamassa molekulaarisessa yksikerroksessa sekä yksikerroksella stabiloiduista kultaklustereista muodostetussa kerroksessa.

Asiasanat Nanopartikkelit, itsejärjestäytyneet yksikerrokset, SECM, molekyylikytkimet

ISBN (painettu)	978-951-22-9361-2	ISSN (painettu)	1795-2239
ISBN (pdf)	978-951-22-9362-9	ISSN (pdf)	1795-4584
Kieli	Englanti	Sivumäärä	68 s. + 44 s.

Julkaisija Kemian laitos

Painetun väitöskirjan jakelu Kemian laitos

☒ Luettavissa verkossa osoitteessa http://lib.tkk.fi/Diss/2008/isbn9789512293629/

Preface

The research presented in this doctoral thesis was carried out at the Laboratory of Physical Chemistry and Electrochemistry, Helsinki University of Technology between January 2005 and February 2008. A period of four months in spring 2005 was spent at the University of Valencia. The work was financially supported by the Kemira foundation and the European Commission.

First, I would like to express my gratitude to my supervisor Prof. Kyösti Kontturi and all the co-authors of the publications included in this thesis. Special acknowledgements go to Prof. David J. Schiffrin for sharing priceless pieces of his experience and to Dr. Timo Laaksonen for giving his great support during this time. Also Dr. Bernadette M. Quinn, Dr. Virginia Ruiz, Dr. Peter Liljeroth, Dr. Christoffer Johans, Antti Nykänen, Prof. Janne Ruokolainen and Dr. Jerzy Paprotny are to be acknowledged for their contribution to this thesis. I would like to thank Dr. Lasse Murtomäki for teaching me the basic knowledge on physical chemistry, Prof. José Manzanares for hosting my stay in Valencia, Hannu Revitzer for making the chemical analysis in some of the studies and Dr. Benjamin Wilson for proof-reading the manuscript of the thesis.

The whole group of researchers, teachers, students and other members of FyKe have earned my compliments for the atmosphere they have created to the laboratory. The discussions and support from the fellow members of FyKe has really made the time spent at the Laboratory of Physical Chemistry and Electrochemistry worth remembering. Finally, I thank my family and friends for supporting me in my choices and their endless patience with me.

This thesis was made out of enthusiasm for research and science.

Päivi Ahonen

Espoo, February 12th, 2008

Table of Contents

List of Publications

This thesis consists of an overview and the following publications which are referred to in the text by their Roman numerals.

I P. Ahonen, T. Laaksonen, A. Nykänen, J. Ruokolainen and K. Kontturi, Formation of Stable Ag-Nanoparticle Aggregates Induced by Dithiol Cross-Linking, *Journal of Physical Chemistry B*, 2006, **110**(26), 12954-12958.

II T. Laaksonen, P. Ahonen, C. Johans and K. Kontturi, Stability and Electrostatics of Mercaptoundecanoic Acid Capped Gold Nanoparticles with Varying Counter-Ion Sizes, *ChemPhysChem*, 2006, **7**(10), 2143-2149.

III P. Ahonen, D. J. Schiffrin, J. Paprotny and K. Kontturi, Optical Switching of Coupled Plasmons of Ag-Nanoparticles by Photoisomerisation of an Azobenzene Ligand, *Physical Chemistry Chemical Physics*, 2007, **9**(5), 651-658.

IV P. Ahonen, T. Laaksonen, D. J. Schiffrin and K. Kontturi, Photoswitching Electron Transport Properties of an Azobenzene Containing Thiol-SAM, *Physical Chemistry Chemical Physics*, 2007, **9**(35), 4898-4901.

V P. Ahonen, V. Ruiz, K. Kontturi, P. Liljeroth and B. M. Quinn, Electrochemical Gating in Scanning Electrochemical Microscopy, *Journal of Physical Chemistry C*, 2008,**112**(7), 2724-2728 .

Author's contribution

Päivi Ahonen has planned and carried out all the experimental work in publications I, III and IV, apart from the synthesis of azobenzene derivatives. Ahonen corresponded also for all theoretical work in publications III and IV. Publication II was planned in collaboration with T. Laaksonen. In publication V, Ahonen carried out the experimental work planned in collaboration with the other authors. Ahonen was actively involved in preparation and writing of each manuscript.

Professor Kyösti Kontturi
Espoo, February 12th, 2008

List of Abbreviations

CCC	Critical coagulation concentration
DLS	Dynamic light scattering
DLVO	Derjaguin-Landau-Verwey-Overbeek theory
DNA	Deoxyribonucleic acid
FcMeOH	Ferrocenemethanol
$FcTMA^+$	Ferrocenetrimethylammonium
MPC	Monolayer protected cluster
MSA	Mercaptosuccinic acid
MUA	Mercaptoundecanoic acid
NC	Nanocluster
NP	Nanoparticle
PET	2-phenylethylthiol
SAM	Self-assembled monolayer
SECM	Scanning electrochemical microscopy
SERS	Surface enhanced Raman scattering
STM	Scanning tunneling microscopy
TBA	Tetrabutylammonium
TEA	Tetraethylammonium
TMA	Tetramethylammonium
UME	Ultramicroelectrode
UV-vis	Ultraviolet and visible light

List of Symbols

α_i	Polarisability of species i
β	Decay constant
$\Gamma(r)$	Radius dependant relaxation constant
Γ_∞	Bulk relaxation constant
$\Gamma_{+/-}$	Eigenvalue of the aggregate mode
Δz	Thickness of the film
$\varepsilon(\omega)$	Dielectric function
ε_0	Permittivity of vacuum, 8.854×10^{-12} Fm^{-1}
$\varepsilon_1(\omega)$	Real part of the dielectric function
$\varepsilon_2(\omega)$	Imaginary part of the dielectric function
$\varepsilon_{\mathrm{bulk}}(\omega)$	Bulk dielectric function
ε_{m}	Dielectric constant of the embedding medium
η	Viscosity; polarisability of a nanoparticle
κ	Inverse Debye length
Λ	Dimensionless kinetic parameter
λ	Wavelength of light
μ	Electrochemical potential
$\tilde{\mu}$	Dimensionless electrochemical potential
μ_{eq}	Equilibrium electrochemical potential
μ^0	Standard electrochemical potential
Σ	Dimensionless conductivity
σ	Conductivity
$\sigma\Delta z$	Conductance
ψ^0	Surface potential
ω_{p}	Plasmon frequency
A	Correction factor for relaxation constant
a	Nanoparticle radius
A_{H}	Hamaker's constant

C_i	Dimensionless concentration of species i
C_{abs}	Absorption cross-section
C_{ext}	Extinction cross-section
C_{sca}	Scattering cross-section
C_i^{b}	Dimensionless bulk concentration of species i
c_i	Concentration of species i
c^{b}	Total bulk concentration
c_i^{b}	Bulk concentration of species i
D	Nanoparticle diameter
D_{i}	Diffusion coefficient of species i
d	Center-to-center particle separation
e	Elementary charge, 1.602×10^{-19} C
E^0	Standard potential
E_{eq}	Equilibrium potential
F	Faraday constant, 96485 Cmol^{-1}
h	Surface-to-surface particle separation
I	Current
i	Dimensionless current
I_{lim}	Limiting current
$I_{\mathrm{T}}^{\mathrm{C}}$	Tip current for a conductive substrate
$I_{\mathrm{T}}^{\mathrm{ins}}$	Tip current for an insulating substrate
$I_{\mathrm{T}}^{\mathrm{k}}$	Tip current
J_i	Diffusion flux of species i
k_{B}	Boltzmann constant, 1.381×10^{-23} JK^{-1}
k_{ET}	Rate constant of electron transfer
K_{eff}	Dimensionless effective rate constant
k_{eff}	Effective rate constant
K^0	Dimensionless standard rate constant
k^0	Standard rate constant
L	Dimensionless tip-substrate separation

m_{e}	Effective mass of electron
N	Density of electrons
$\tilde{N}(\omega)$	Complex refraction index
N_A	Avogadro's number, $6.022 \times 10^{23}\ mol^{-1}$
n_{m}	Refractive index of the embedding medium
R	Ideal gas constant, 8.314 $\mathrm{Jmol^{-1}K^{-1}}$; dimensionless radial distance
RG	Dimensionless electrode shape factor
r	Radius; radial variable
r_{e}	Radius of the electrode
r_{g}	Total radius of the electrode including the glass sheath
T	Temperature; dimensionless time
t	Time
V_{attr}	Attractive potential
V_{rep}	Repulsive potential
v_{F}	Fermi velocity
Z	Dimensionless distance normal to the electrode surface
z	Distance normal to the electrode surface; number of electrical charges

1 Introduction

Self-assembly of chemical structures has attracted a great interest throughout the history of nanotechnology. Good examples of self-assembled systems are biological forms like cell membranes where the lipids assemble due to amphiphilic and steric interactions and form a bilayer able to support the interiors of the cell. Similar spontaneous self-assembly has been applied in nanotechnology to form new structures and the principle is commonly called the 'bottom-up' approach. In this thesis, simple metal nanoparticle superstructures and molecular monolayers formed by the bottom-up approach are investigated. The formation and fundamental properties of single nanoparticles are not the focus of this thesis, but the interest is on assemblies formed of numerous particles and their properties. The emphasis is on controlling the optical and electrical interactions between the nanoparticles embedded in the superstructures, for instance by changing the conformation of the superstructure in a controlled way. In addition, changes in the interparticle interactions lead to changes in the properties of the whole superstructure.

The collective properties of metal nanoparticle superstructures have been applied in the development of different types of sensors. Sensors based on films of nanoparticles linked to each other are typically chemiresistors, with their conductance dependant on the adsorption of certain chemical species into the film. [1] These kinds of sensors may also be used as colourimetric sensors, if the sensing is based on changes in interparticle distances, which also has an effect on the optical properties of the nanoparticle assemblies. [2] Another sensor type is based on the enhancement of the signal due to electrical or optical properties of the nanoparticles, e.g. surface enhancement of Raman scattering (SERS) near nanopatterned silver surfaces. [3] SERS is based on the strong local electromagnetic field near the surfaces of periodic nanostructures and allows even single molecule detection. Yet another type of signal magnification occurs in hybrid materials consisting of biomolecules and metal nanoparticles, for example, the signal obtained from a glucose-oxidase enzyme has been enhanced by one order of magnitude. [4] This thesis consists of

studies considering the optical and electrical interactions in assemblies formed of metal nanoparticles, thus introducing some of the fundamental properties behind the function of above mentioned devices.

Metallic nanoparticles do not only provide an inert template for various chemical functionalities but there are peculiar properties embedded in these nanomaterials themselves. [5] The most important properties, specific for metal nanoparticles, are their low melting temperature (thermodynamic properties) [6], surface plasmon absorption (optical properties) [7], room-temperature quantised charging (electrical properties) [8], catalytic [9] and magnetic properties. [10] Also interesting are the interparticle interactions and their effects on the superstructure properties. In this thesis, a series of physicochemical studies on the collective optical and electrical properties of superstructures consisting of silver and gold nanoparticles are presented.

The first chapter considers the formation of colloidal nanoparticle superstructures driven by the interaction between the individual nanoparticles. Aggregation of nanoparticles is induced by either chemical (publication I) or electrostatic (publication II) interactions. The nature of the interaction affects both the time-scale of the superstructure formation and the final structure of the aggregate. [11] On the other hand, the coagulation of the nanoparticles is often unwanted and thus the basic knowledge of the cluster formation process is necessary.

The second part of this work introduces the basis for the optical properties of both single nanoparticles and interacting particle clusters. The optical spectrum of silver nanoparticles and nanoparticle clusters are examined in order to explain the changes in plasmon absorption arising from the particle-particle interaction. In publication III, a photoresponsive nanoswitch is built from silver nanoparticles and azobenzene functionalised molecules. The most studied applications of the plasmonic coupling of nanoparticles are different types of sensors [12] and the phenomena they are based on, are described in this section.

The third part of the thesis is about the electrical properties of nano-scale films and application of scanning electrochemical microscopy (SECM) [13] on studying

them. Two different approaches are presented; the first one (publication IV) shows how to characterise and manipulate barrier properties of a self-assembled monolayer built on Au(111) surface. The second approach (publication V) presents a study of lateral conductivity of a film consisting of gold nanoclusters. The uniqueness of the latter study is on controlling the film potential without electrical contacts.

Before closing the introductory section, the rather broad concept of a nanoparticle needs to be clarified. Any particle from a metallic nanocrystal to biological assembly, such as a liposome, having a size in the nanometre scale, can be considered as a nanoparticle. In this thesis however, the term nanoparticle has been used exclusively to address particles having a metallic core and a capping monolayer of some ligand surrounding the surface. [5, 8] In publications I, II and III the particles having 3-4 nm diameters have been called simply 'nanoparticles' (NPs), whereas the very small particles having a well defined core structure in publication V have been referred to as either 'monolayer protected clusters' (MPCs) or 'nanoclusters' (NCs). [8, 14, 15]

2 Colloidal nanoparticle superstructures via self-assembly

2.1 Dithiol induced nanoparticle cluster formation

Nanoparticles and especially architectures constructed from nanoparticles are of great interest for the possibility of making nanoscale devices by self-assembly techniques. [2, 16–19] A well known method to form self-assembled nanoparticle structures is to cross-link nanoparticles with α,ω-functionalised ligands [20], such as dithiols (see figure 2.1). Materials formed in this way maintain many of the unusual properties of their original nanosized components because the MPCs remain segregated. [18, 21] Some of the properties depend on the particle-particle separations and are thus tunable, because the distance separating the particles is well defined by the choice of the linker molecule. Both noncovalent [22–31] and covalent [1, 32–46] thiol-bonding induced self-assembly of nanoparticles has been studied widely, with most of the published work focussing on the electrical and optical properties of the nanoparticle materials formed.

In publication I, aggregation of thiol stabilised 2.9 nm silver nanoparticles induced by 1,6-hexane dithiol (figure 2.1 b) was studied by dynamic light scattering (DLS). While *in situ* observation of direct thiol exchange seems unreachable, aggregation caused by cross-linking of nanoparticles can easily be monitored. By linking the aggregation rate of the nanoparticles to the rate of the thiol exchange reaction on their surfaces, the kinetics of the thiol exchange can be probed indirectly with DLS. Another way to study formation of nanoparticle clusters would be to monitor their size microscopically, where samples must be taken and the reaction quenched at appropriate time intervals. With DLS, one can follow the evolution of colloid size in the same sample without the tedious work required to prepare one sample for each time step. The reaction scheme for the aggregation process is presented in figure 2.2. (Assumptions of the model are discussed in more detail later on in this section.)

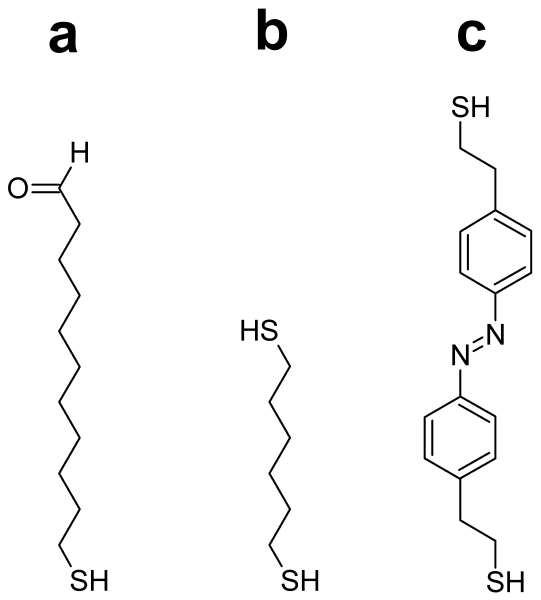

Figure 2.1: Examples of α,ω-functionalised molecules. (a) Mercaptoundecanoic acid, (b) 1,6-hexanedithiol and (c) azobenzene derivatised dithiol (AZO2)

DLS measures the diffusion motion of the clusters, allowing the measurement of the diffusion coefficient, from which the hydrodynamic radius can be extracted. In publication I, an instrument based on the backscattering of light from the sample was employed. Collecting the back scattered light avoids multiple scattering from the particles and facilitates the measurement of strongly absorbing colloids. For small metallic nanoparticles (diameter < 10 nm), absorption dominates the extinction spectrum (see section 3.2), which lowers the intensity of scattered light and causes difficulties in conventional light-scattering measurements. With instruments based on back scattering one can characterise sizes even smaller than 2 nm. [47, 48] Another advantage of measuring back scattered light is the non-destructive nature of the method compared to the conventional light scattering measurements. The interaction between the nanoparticles and the 633 nm laser of the DLS instrument was neglected, since the dodecanethiol capped silver nanoparticles employed in the measurements do not absorb light at this particular wavelength.

In all of the measurements (figure 2.3), a rapid growth stage followed by lev-

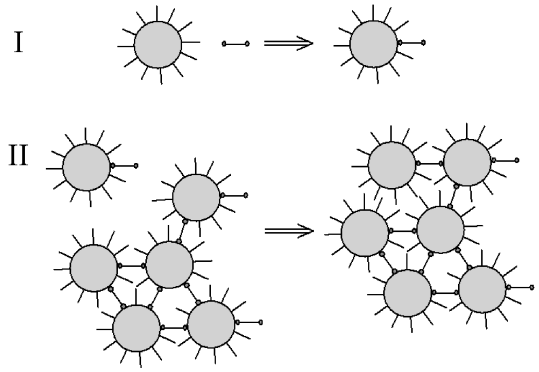

Figure 2.2: A reaction scheme describing the two-step reaction of the nanoparticles and dithiols. In phase I, thiol-functionalised nanoparticles are formed. In phase two, the functionalised particles react further with the other functionalised particles thus forming an aggregate. (Reprinted with permission from The American Chemical Society)

elling out of the hydrodynamic radius was observed. After 60 minutes, a stable size was reached when the solution was depleted of nanoparticles. The final hydrodynamic radius was between 100 and 160 nm in all of the measurements. This size did not change noticeably even after 24 hours, indicating that aggregates do not have the tendency to coalesce to form larger structures in the time-scale considered.

A monomer-aggregate growth mechanism was assumed to allow the application of a mathematically simple model. In the model, dithiol-functionalised particles are denoted as the monomers, which are attached to the aggregates, thus forming larger nanoparticle clusters (see figure 2.2). According to the Fick's first law, the diffusion flux J_i of a species in spherical coordinates is defined as the product of the diffusion coefficient D_i and the concentration gradient of the species.

$$J_i = D_i \frac{dc}{dr} \tag{2.1}$$

When comparing the fluxes of the individual nanoparticles and the nanoparticle clusters, the ratio of the fluxes stays rather high throughout the whole experiment, because of the slow diffusion of the large clusters. In addition the number of clusters

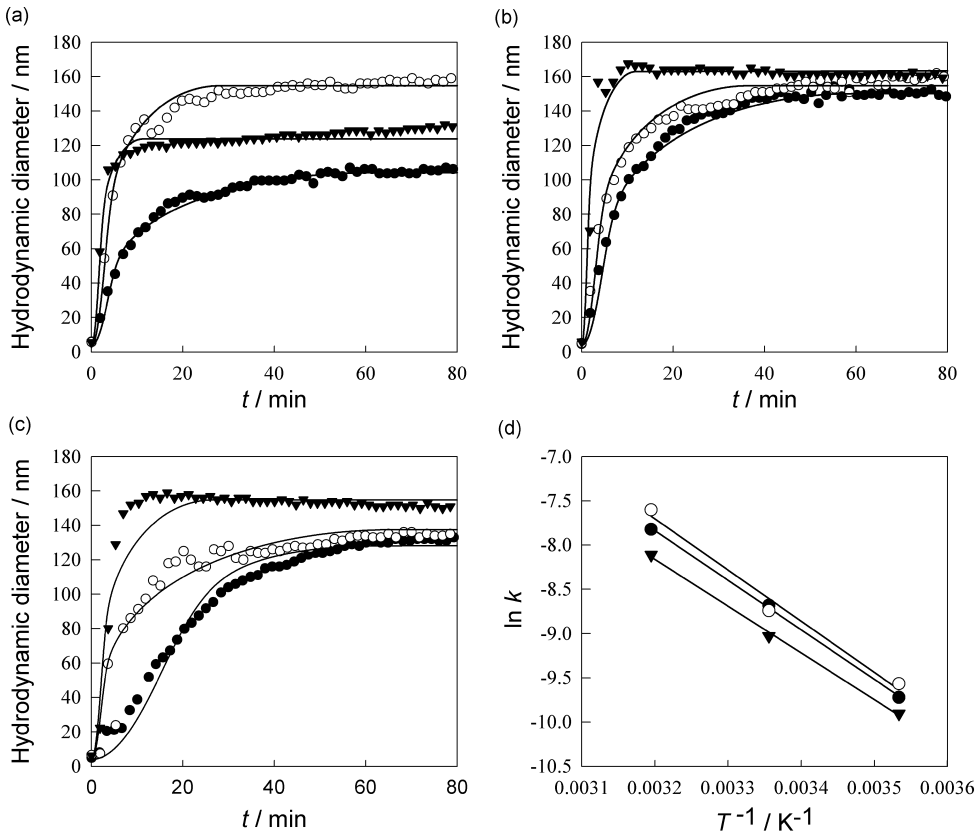

Figure 2.3: Evolution of the hydrodynamic radius of the nanoparticle aggregate: experimental results (dots) and calculated values (solid lines). The dithiol:NP ratio was 94 (a), 47 (b) and 9 (c). Temperature was set to 10 ℃ (filled circles), 25 ℃ (open circles) and 40 ℃ (triangles). Arrhenius plot (d) is shown for the same calculations. The dithiol:NP ratio was 94 (triangles), 47 (open circles) and 9 (filled circles). (Reprinted with permission from The American Chemical Society)

is assumed to be constant throughout the experiment and thus, it is much lower than the number of single nanoparticles at the beginning of the experiment and the growth by combination of aggregates can be neglected. The combination of aggregates over a longer time-scale was not part of this study. Dependence of the diffusion coefficient on the cluster/aggregate size can be approximated from Stokes-Einstein relation (equation 2.2), where k_{B} is the Boltzmann constant, T is the temperature, η is the viscosity of the medium and r is the radius of the particle. From this relation, corresponding radii values for measured diffusion coefficients can be obtained. The

values of diffusion coefficients of single nanoparticles with ~ 3 nm radii are the order of 10^{-6} cm^{2}s^{-1} whereas for nanoparticle clusters of 150 - 200 nm in diameter they are two orders of magnitude lower.

$$D = \frac{k_{\mathrm{B}}T}{6\pi\eta r} \tag{2.2}$$

Furthermore, all aggregates are assumed to be spherical and of the same size. While there certainly will be a distribution in size, this assumption simplifies the model greatly and reduces the number of parameters required. As mentioned above, simultaneous nucleation meaning a fixed number of nucleation points throughout the experiment was assumed. A detailed description of the model is presented in publication I.

Despite all the simplifications, the model shows a good correlation with the measured data. The rate constants for the thiol exchange, monomer desorption and adsorption were used as the free parameters in fitting. Values corresponding to monomer attachment and desorption were found to have only a minor effect on the shape of the fitted curves and thus could not be fitted accurately. However, the rate constant for the apparent thiol exchange reaction was found to vary between 0.6 and 4.0×10^{-4} s^{-1} and to follow the Arrhenius equation, from which the activation energy of 46 ± 10 kJ mol^{-1} was calculated (figure 2.3 d).

To conclude publication I, new information of the formation of stable clusters of thiol capped silver nanoparticles could be obtained by measuring the evolution of aggregate size with dynamic light scattering. Under diffusion control, stable aggregates of around 140 nm were reproducibly obtained via dithiol cross-linking of the nanoparticles. The main objective of the study was to obtain kinetic information about the thiol exchange reaction from an approach that combines the growth process of a nanoparticle superstructure to the functionalisation of the nanoparticles with dithiol molecules. The main assumptions in the model were that the reaction is considered to proceed with dithiol-functionalised nanoparticles attaching to a growing nanoparticle cluster and that the cluster-cluster growth does not occur in the

same time-scale. In summary, we have demonstrated that dynamic light scattering provides a simple and effective means of probing the kinetics of place-exchange reactions on nanoparticle surfaces.

2.2 Enhancing the stability of aqueous nanoparticle colloids

In water, coagulation of colloidal nanoparticles typically occurs due to the electrostatic interaction between the nanoparticles' ligand shells or their complexation to each other. [24] Among the most studied applications for nanoparticle coagulation are sensors, where the aggregation process of nanoparticles is induced by DNA- [49–52] or other molecule recognition. [53,54] Aggregation for instance, causes changes in the optical spectrum of the particles and increases electrical conductivity of a particle assembly (discussed in sections 3.2 and 4.2), which gives a way to monitor specific interactions between molecules and nanoparticles. However, in many cases, coagulation of the nanoparticles is not desirable and ways to avoid it are needed. For instance, when studying the properties of individual nanoparticles, the collective behaviour of nanoclusters in aggregates may affect the observed properties. Also when using nanoparticles in biological systems, for instance for target amplification in biochips, [55, 56] non-specific coagulation is unwanted.

Typically small water-soluble nanoclusters are capped with carboxylic acid terminated ligands and their solubility is highly dependant on the solution they are immersed in. At low pH, the nanoparticles agglomerate due to protonation and hydrogen bonding. [57] At high pH, the acid groups deprotonate and stabilise the particle dispersion through electrostatic repulsion and prevent the aggregation of the particles. Overlapping of the electrical double layers surrounding the particles prevents them from approaching each other and agglomerating by attractive van der Waals forces, thus determining the distance of closest approach of the nanoparticles. The thickness of the electrical double layer surrounding the particles depends on the salt concentration of the solution and a schematic of the structure of the electrical double layer for a acid-capped nanoparticle is shown in figure 2.4.

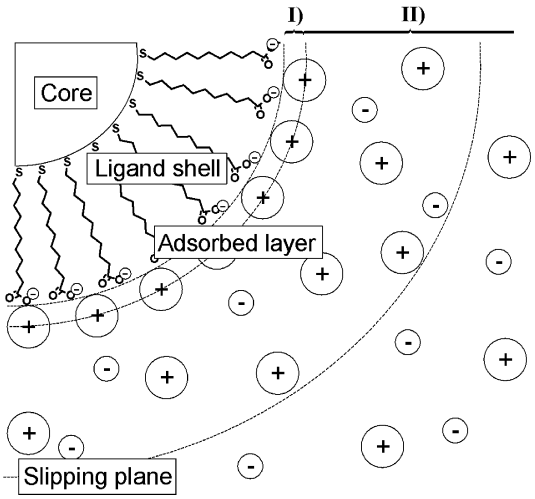

Figure 2.4: Structure of the electric double layer at the surface of a nanoparticle capped with mercaptoundecanoic acid. (Reproduced with permission from Wiley-VCH Verlag GmbH & Co. KGaA)

It is well known that the electrical double layer surrounding a colloid contracts as the salt concentration of the embedding solution increases. When the ionic strength exceeds a limit known as the critical coagulation concentration (CCC), the double layer is contracted so much and the surface potential decreased to so low that the colloidal particles coagulate. [58] This limit is strongly dependant on the charge of the counter-ion [59] and to a lesser extent on the structure and size of the ion. Typically the critical concentration is much lower for multivalent counter-ions [59] than for univalent counter-ions. A common theory for describing the stability of colloidal systems of this type is the Derjaguin-Landau-Verwey-Overbeek (DLVO) theory [11, 59], which works well in a qualitative manner for most systems, but needs modifications at very small length scales. [60, 61]

The role of the electric double layer structure in the stability of colloids is of major importance. [62] The focus of publication II was to study the effect of different sized ions on the position of the so called slipping plane (see figure 2.4). The slipping plane includes the volume of specifically adsorbed ions of the Stern layer (Area I in figure 2.4) and the diffusive double layer (Area II in figure 2.4), in

which the distribution of the electrolyte compensates the potential induced by the nanoparticle surface. In practice, the slipping plane includes the electrolyte that moves with the particle, when subjected to external electric field. The potential at the slipping plane is called ζ-potential and is a measurable quantity. In publication II, the stability of mercaptoundecanoic acid (MUA, see figure 2.1) capped Au-nanoparticles in the presence of different ions was studied. Hydroxides with different sized cations were used to set the pH to the range where the particles were soluble in water. Counter-ions used were sodium (Na^+) and three different quaternary ammonium ions; tetramethylammonium (TMA^+), tetraethylammonium (TEA^+) and tetrabutylammonium (TBA^+), which have radii of 0.95, 2.85, 3.48 and 4.37 Å respectively. The size of the counter ion was assumed to change the distance of closest approach of the nanoparticles, thus affecting their tendency to coagulate.

Stability of the nanoparticles in aqueous solutions with varying ion strengths and counter-ions was determined by measurement of the particle sizes by DLS and by analysing the double layer structure from the measured ζ-potentials. With Na^+ as the counter-ion, the particles precipitated in the concentration range of 70 - 90 mM, whereas with quaternary ammonium hydroxides the particles were stable even in concentrations exceeding 1 M. The increased concentration range obtained with TEAOH was also used to facilitate thiol exchange between MUA and mercaptosuccinic acid (MSA) at the nanoparticle's surface. In a basic solution, with rather low salt concentrations, the electrostatic repulsion between the monovalent MUA and bivalent MSA would be very high and no place-exchange reactions would occur. By increasing the salt concentration of the solution, the surface potential of the nanoparticles could be lowered and thus the place-exchange could proceed. By using TEAOH, the ligand exchange could be facilitated to an extent, which would have been impossible to do in NaOH solutions.

The interactions between the colloidal particles was approximated with the simple DLVO theory. Total interaction potential was assumed to be the linear superposition of the repulsive and attractive potentials. [62] Repulsive potential was calculated from the electrostatic repulsion between two charged particles: [63]

$$V_{\mathrm{rep}} = 4\pi a^2(\psi^0)^2\Big(\frac{RT}{F}\Big)^2\frac{e^{-\kappa h}}{2a+h} \tag{2.3}$$

where a is the radius of a particle, ψ^0 is the surface potential, R is the gas constant, T is the absolute temperature, F is the Faraday constant, κ is the reciprocal Debye length and h is the surface-to-surface separation of the nanoparticles. The electrostatics of the colloidal nanoparticles are discussed further in Publication II, where an approximation of the potential distribution surrounding the nanoparticle is derived in detail.

The attractive potential between the particles was calculated from the attractive van der Waals forces:

$$V_{\mathrm{attr}} = -\frac{A_{\mathrm{H}}}{6}\left[\frac{2a^2}{h^2+4ah} + \frac{2a^2}{(h+2a)^2} + \ln\frac{h^2+4ah}{(h+2a)^2}\right] \tag{2.4}$$

where A_{H} is the Hamaker constant describing the dielectric properties of the dispersant and the particles. The value 4.53×10^{-19} J (corresponding to 100 $k_{\mathrm{B}}T$) was used for the gold nanoparticles. [64] Simulations showing the interaction energy of two spherical particles as a function of the distance between the particles are plotted in figure 2.5. The salt concentration of the solution is varied and a significant decrease in the interaction energy is seen as the concentration is increased. Finally, all the repulsive interactions are lost as concentration exceeds 1 M. This means that according to DLVO theory, in electrolyte concentrations exceeding 1 M, the colloid is no longer stable but some interaction at molecular level, such as a specifically adsorbed layer of ions, results in extra colloid stabilisation. Since the colloid stability increases as the counter ion size increases, the extra stabilisation is probably due to steric effects.

As demonstrated in publication II, the choice of electrolyte should be carefully considered when using this type of nanoparticles in aqueous environments, especially in biological systems. This study widens the use of metallic nanoparticles as labels in DNA recognition, since the electrolyte concentrations in biological systems range

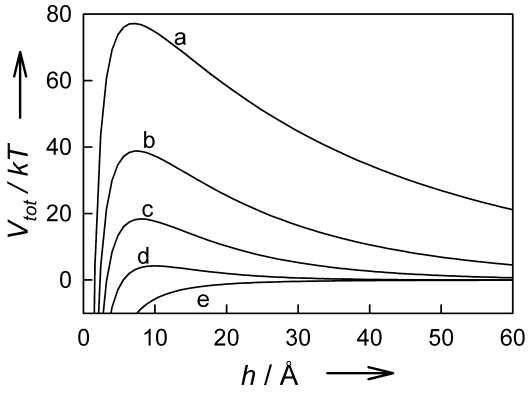

Figure 2.5: Simulated interaction energy between two spheres in different salt concentrations. (a) 1 mM, (b) 10 mM, (c) 30 mM, (d) 90 mM and (e) > 1 M. (Reproduced with permission from Wiley-VCH Verlag GmbH & Co. KGaA)

over several hundreds of mM rather than below 100 mM, which is the CCC limit determined for NaOH. A simple modification of the system gives greatly enhanced stability and even allows surface reactions that would otherwise not proceed. This study shows the advantage of multidisciplinary physichochemical approach on a matter of great interest to both chemists and biologists.

3 Building a nanoswitch via self-assembly of nanoparticles

3.1 Photoisomerisation of azobenzene derivatised silver nanoparticles

Molecules having bistable nature are often considered as molecular switches. In order to work as a switch, a molecule has to have a reversibly switching property controllable by external stimuli. A typical example of a molecular switch is a photoisomerisable molecule, whose conformation can be varied between two stable states, e.g. *trans* and *cis* states. The actual property changed in the isomerisation reaction is the conformation of the molecule but also changes in the molecular conductance can occur simultaneously (discussed in detail in chapter 4.1). [65–67] Several types of molecular switches including those based on changes in conformation or conductance [68–71] have been recently described.

Azobenzene compounds have gained much attention because of the ability to control both the conformation [67] and conductance [66] of the molecule by photoisomerisation. Light energy is transformed to mechanical work in the photoisomerisation process of the azobenzene group. [72] Although the photoisomerisation reaction has been known for a long time, the excitation mechanism and optical properties of the azobenzene chromophore are still under investigation. [73, 74] The azobenzene group is isomerised from the more stable *trans* to the *cis* ground state by UV light of 366 nm and back to the trans conformer with blue light or thermal relaxation (See figure 3.1). [75] The photoswitchable azobenzene moiety has been utilised, for instance, in controlling the properties of functional polymeric materials [76], in data storage [77, 78] and other self-assembling systems. [39, 79]

In publication III, photoisomerisation of azobenzene molecules attached to silver nanoparticles via thiol bonding was studied. The aim was to find out if any interactions between the chromophore and the nanoparticle occur during the photoisomerisation process. It was assumed that transfer of energy between the

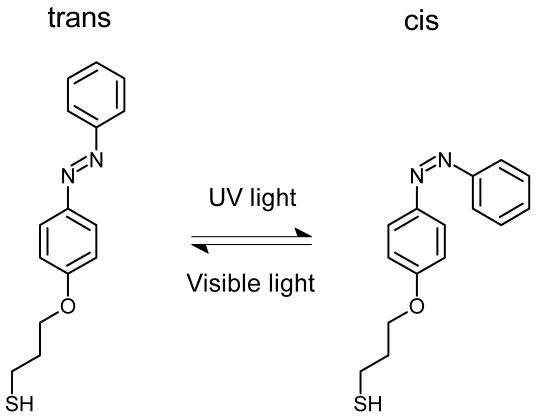

Figure 3.1: Photoisomerisation reaction of an azobenzene derivatised thiol (AZO1).

azobenzene group and the nanoparticle brought to very close proximity could occur because the molecular orbital of azobenzene overlaps with the plasmon band of the Ag-nanoparticles. The concept of the plasmon band is clarified in chapter 3.2. Photoisomerisation was followed by UV-vis spectrometry, since *trans* and *cis* isomers of azobenzene absorb UV and visible light at different wavelengths (figure 3.2 a). Spectra of the *trans* and *cis* isomers of the azobenzene monothiol AZO1 (figure 3.1) free in toluene solution and attached to the 3.7 nm Ag-nanoparticles were recorded and a comparison made (figure 3.2). A difference in the spectral changes during the photoisomerisation was observed around the plasmon absorption wavelength ($\sim$ 460 nm) of thiol capped silver nanoparticles, which was considered as evidence of interaction between the azobenzene chromophore and the nanoparticle.

The intensity of the plasmon band of the functionalised nanoparticles decreased as the azobenzene derivatised ligand was photoisomerised from *trans* to *cis* state, whereas for the free azobenzene molecule intensity near 440 nm increased as the photoisomerisation occurred. This enhancement of the absorbance of *trans* azobenzene functionalised nanoparticles is likely due to the change in the conductance of the azobenzene ligands through the conformational change. [66] This means that the free electrons of the nanoparticles are spread further from the core when the ligand is in *trans* conformer. Thus, it seems that the *trans* AZO1 can be considered as

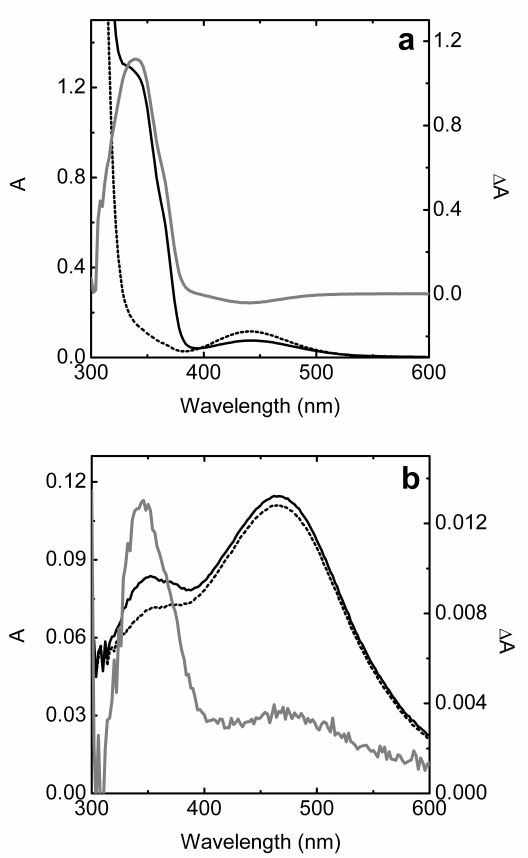

Figure 3.2: (a) Left axis: Spectra of the *trans* conformer (solid black line) and the *cis* conformer (dashed black line) of the free AZO1 in toluene. Right axis: The difference spectrum of the conformers (gray line). (b) Left axis: Spectra of silver nanoparticles functionalised with *trans* AZO1 (solid black line). Spectrum after photoisomerisation of the ligand to the *cis* conformer (dashed black line). Right axis: The difference spectrum of the azobenzene functionalised nanoparticles (gray line).

an antenna when attached to the surface of a Ag-nanoparticle and by changing the state of AZO1, the dielectric properties of the nanoparticle can be tuned by light. As a conclusion, by attaching an interacting switchable molecule to a nanoparticle, it is possible to turn the whole nanoparticle into a switch.

3.2 Optical properties of nanoparticle clusters at quasi-static region

In this section a survey of the optical properties of superstructures consisting of metallic nanoparticles is made. Simplified approximations describing the UV-vis spectrum of a silver nanoparticle and a nanoparticle pair are derived. In addition, the effect of the interparticle distance of the nanoparticles on the optical response of these superstructures is discussed. In publication III, clusters of silver nanoparticles were formed by cross-linking the particles with an azobenzene containing dithiol. The effect of photoisomerisation of the linker molecule on the structure of the formed superstructures was analysed from UV-vis spectra. Measured changes were then compared to the above mentioned model to extract the result of photoisomerisation in the interparticle distance of the nanoparticles.

A theory that considers scattering and absorption of light by small spherical particles is based on classical electrodynamics and was first published by Mie in 1908. [80] Mie theory provides an exact result for scattering and extinction cross-sections, from which the absorption cross-section can be calculated:

$$C_{\text{ext}} = C_{\text{abs}} - C_{\text{sca}} \tag{3.1}$$

Similar models involving different particle geometries have also been derived. [81,82] The major problem of the classical theories is the dependence of the optical constants on the wavelength of light. This means that a complex dielectric function of the particles must be known. The generalised form of the complex dielectric function is presented in equation 3.2:

$$\varepsilon(\omega) = \varepsilon_1(\omega) + i\varepsilon_2(\omega) = \left(\tilde{N}(\omega)\right)^2 \tag{3.2}$$

where ε_1 and ε_2 are the real and imaginary parts of the dielectric function respectively. The relation between the dielectric function and the complex index of refraction, $\tilde{N}$, is also expressed in the equation. The problem of finding the correct dielectric function for nanosized objects is significant, since below a certain size limit, the dielectric function becomes size-dependant and thus deviates from the bulk properties. Modification of the bulk dielectric function has been considered in the literature, for instance, by taking into account the reduced mean free path of the electrons, the spill-out of electrons and development of the dielectric function from a quantum-mechanical point of view. [7]

When looking for a suitable form of the dielectric function for very small particles, some simplifications to the mathematical treatment can be made. When comparing nanoparticles below 10 nm in diameter to the wavelength of visible light, it can be shown, that the particles are so small that there are no fluctuations of the electromagnetic field due to the presence of the nanoparticles. This is called the quasi-static approximation and it applies to every wavelength where $\lambda >> r$ and is widely used in the modelling of small clusters. [7, 82]

In metal and semiconductor crystals there are electrons that can be considered to move rather freely in the crystal lattice and free electrons respond to the oscillation of an external electromagnetic field in a collective way. The wavelength at which the free-electron plasma resonates is called the plasmon resonance and its wavelength depends on the material and the environment of the particle. The contribution of the free electrons and the electrons bound to the crystal lattice to the optical spectrum can be distinguished from each other so that the plasmon resonance phenomenon can be examined independently from the quantum-mechanical contributions of the metal core. [83] For some transition metal nanoparticles, like gold, silver and copper, plasmon resonance appears in the visible region of wavelengths and can be observed as an absorbance band in the optical spectrum. [7] The

angular frequency of the surface plasmon ω_p of a free-electron metal, such as silver, can be approximated from the following equation: [84]

$$\omega_\mathrm{p} = \sqrt{\frac{Ne^2}{\varepsilon_0 m_\mathrm{e}}} \tag{3.3}$$

where N is the density of electrons, e is the elementary charge, ε_0 is the permittivity of vacuum and m_e is the effective mass of an electron. The real position of the plasmon absorption of colloidal nanoparticles differs from this approximation because here only free-electron contributions are considered and the effects of size and geometry have not been taken into account. [85, 86] The layer of the capping ligand also shifts towards higher wavelengths and dampens the plasmon band of individual nanoparticles. [84, 87]

When two particles are brought to a short enough distance from each other, the plasmon resonances of individual particles couple. [2, 24, 88, 89] This coupling is seen as a longitudinal plasmon band at a higher wavelength, i.e. lower in energy, than the primary plasmon resonance. An approximation of the optical spectrum of two attached nanoparticles can be calculated using a simplified model describing the vibrational coupling of plasmon resonances of two clusters in close proximity. [7, 82, 90] This model takes into account the changes in the local field near the neighboring clusters due the irradiation by light. It is assumed that no tunneling of electrons occurs between the clusters, which means that the clusters remain electrically isolated in the aggregates.

In Publication III, Drude-theory was used as the starting point for modelling the complex dielectric function (equation 3.4). Drude-theory considers only free-electron contributions in metals, which means that the response to the electromagnetic field is mainly due to the transitions of the electrons in the conduction band, i.e. intraband transitions. [7] Drude-theory is applicable for nanoparticles made of alkali metals and some noble metals like silver and it was chosen here for its simplicity. [7] However, the dielectric function of the 3.7 nm silver nanoparticles was corrected by substituting the bulk relaxation constant Γ_∞ in the Drude dielectric

function with a radius dependant quantity $\Gamma(R)$ (equation 3.5). [7, 91] This correction is called the free-path effect and it is based on the fact that the nanoparticle dimensions are smaller than the mean free-path of electrons in bulk metal. Thus the size of the nanoparticle is actually restricting the movement of electrons in the nanoparticle.

$$\varepsilon(\omega) = 1 - \frac{\omega_{\mathrm{p}}^2}{\omega^2 + \mathrm{i}\Gamma_\infty\omega} + \mathrm{i}\frac{\omega_{\mathrm{p}}^2\Gamma_\infty}{\omega(\omega^2 + \Gamma_\infty^2)} \tag{3.4}$$

$$\varepsilon(\omega, r) = \varepsilon_{\mathrm{bulk}}(\omega) + \omega_{\mathrm{p}}^2\left(\frac{1}{\omega^2 + \Gamma_\infty^2} - \frac{1}{\omega^2 + \Gamma(r)^2}\right) + i\frac{\omega_{\mathrm{p}}^2}{\omega}\left(\frac{\Gamma(r)}{\omega^2 + \Gamma(r)^2} - \frac{\Gamma_\infty}{\omega^2 + \Gamma_\infty^2}\right) \tag{3.5}$$

where the corrected relaxation constant is:

$$\Gamma(r) = \Gamma_\infty + A\frac{v_{\mathrm{F}}}{r} \tag{3.6}$$

where r is the radius of a nanoparticle, v_{F} is the Fermi velocity in bulk metal. Since the radius of the particles investigated here is smaller than the mean free path in the bulk metal, the particle radius has been taken as the mean free path to calculate the dielectric function of the particles. A is a model-dependant factor and can be taken as 1 for spherical particles. [7] The dielectric function for bulk silver was calculated from optical constants obtained by Quinten. [92] Bulk plasma frequency was calculated from equation 3.3 assuming the effective mass of an electron to be 0.96 times the mass of an electron. [90] Simulated dielectric functions of different sized silver nanoparticles are presented in figure 3.3. The radius of the particles was varied from 1 nm to 10 nm and the bulk dielectric function was plotted as well to illustrate the size effect of the free-path corrected model.

When measuring the optical spectra of nanoparticle superstructures, one often

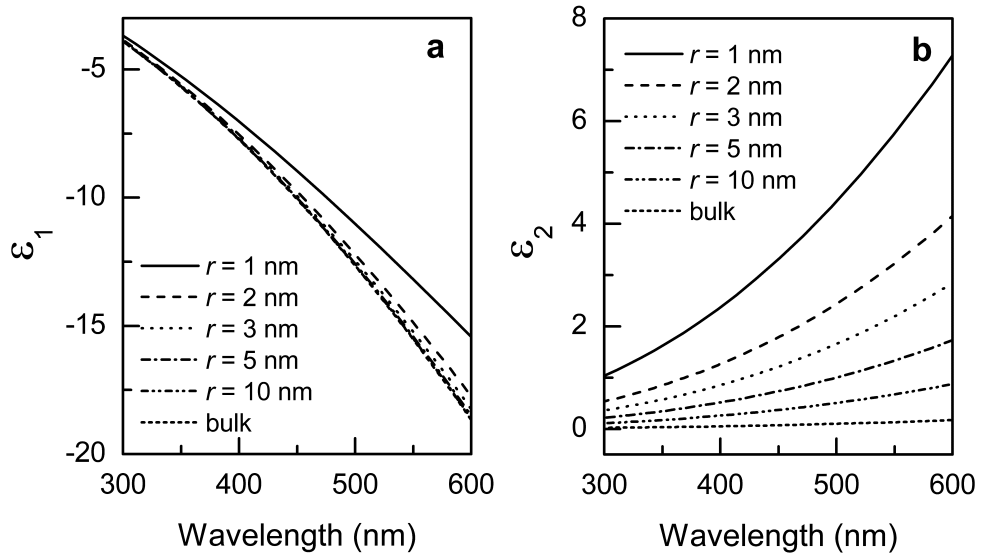

Figure 3.3: Simulated complex dielectric functions for different sized nanoparticles. (a) Real part of the dielectric function and (b) imaginary part of the dielectric function.

observes broadening or even splitting of the original plasmon absorption band into two new bands. This phenomenon is called plasmon coupling and it is due to the electromagnetic interaction between the oscillating plasmas of two nanoparticles when the particles are brought close to each other. The simplest coupled system is a pair of particles with similar dimensions and such a system is considered here. An approximative approach to model the spectrum of a nanoparticle pair is made by considering the coupling of polarisabilities of single nanoparticles. [7] Considering only the transversal and longitudinal in-phase modes of a cluster pair, the component of the aggregate polarisability parallel to the external field of a pair consisting of two particles of equal size is given by:

$$\langle \alpha_{\parallel \mathrm{pair}} \rangle = \frac{8\pi\varepsilon_0\varepsilon_\mathrm{m}\eta r^3}{3}\left(\frac{1}{1+\Gamma_-\eta}+\frac{2}{1+\Gamma_+\eta}\right) \tag{3.7}$$

where ε_m is the dielectric constant of the embedding medium, Γ_+ and Γ_- are the eigenvalues of the aggregate modes and d is the centre-to-centre particle separation.

The polarisability η of a single nanoparticle is defined as:

$$\eta = \frac{\varepsilon(\omega, r) - \varepsilon_{\mathrm{m}}}{\varepsilon(\omega, r) + 2\varepsilon_{\mathrm{m}}} \tag{3.8}$$

According to equation 3.1, the contribution of absorbance to the total extinction spectrum is resolved by subtracting the scattering cross-section from the extinction cross-section. Under quasi-static conditions, the extinction cross-section C_{ext} and scattering cross-section C_{sca} simplify to following forms. [82]

$$C_{\mathrm{ext}} = 2\pi n_{\mathrm{m}} \mathrm{Im}\{\langle \alpha_{\parallel \mathrm{pair}} \rangle\} \tag{3.9}$$

$$C_{\mathrm{sca}} = \frac{8\pi^3 n_{\mathrm{m}}^4}{3} |\langle \alpha_{\parallel \mathrm{pair}} \rangle|^2 \tag{3.10}$$

where n_{m} is the refractive index of the embedding medium, the square root of ε_{m}. Simulations of the spectra of nanoparticle pairs are shown in figure 3.4. The particle-to-particle separations are expressed as the dimensionless ratio of the centre-to-centre distance of the particles to the nanoparticle radius d/D. This ratio was varied from 1.1 to 2.0 for nanoparticle radii 1 nm (figure 3.4 a) and 3 nm (figure 3.4 b). As can be seen, the separation of the two absorption bands, the plasmon band and the longitudinal plasmon band, depends on the distance between the nanoparticles. It has actually been proposed that there is a universal dependence between the band separation and the ratio d/D, which is independent of the absolute size of the particles. [88] On the other hand the intensity of the bands increases by two orders of magnitude as the particle size increases from 1 nm to 3 nm, leading to more intense absorption bands. In figure 3.4 the spectra are presented in normalised form.

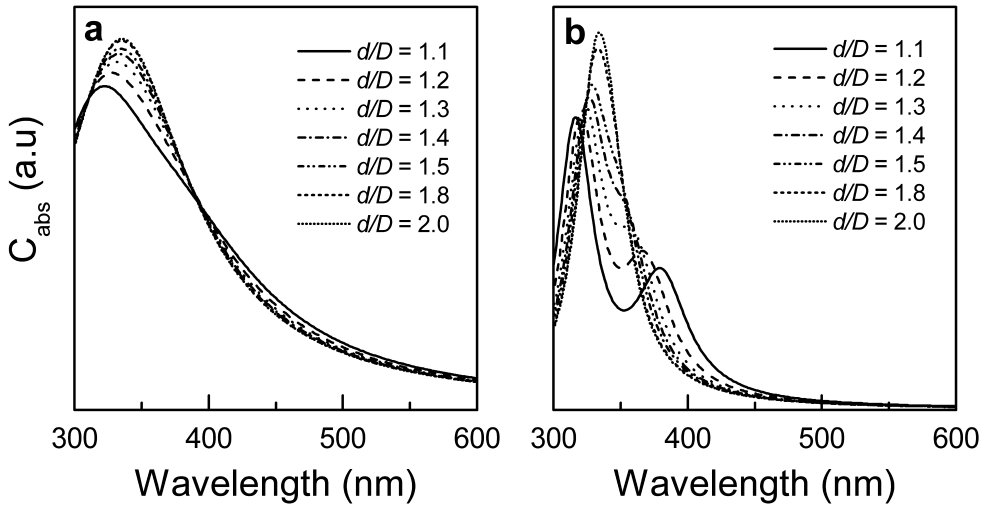

Figure 3.4: Simulated absorption cross-sections of nanoparticle pairs with varying separation/diameter ratios. Particle radii are 1 nm (a) and 3 nm (b). Note that the spectra are presented on arbitrary scale.

3.3 Optical switching of coupled plasmons of Ag-nanoparticles by photoisomerisation of an azobenzene ligand

In publication III, the possibilities of forming switching nanoparticle superstructures by cross-linking them with azobenzene dithiol (AZO2, figure 2.1 c) were studied. The coupling of optical plasmons in nanoparticle aggregates depends critically on the interparticle distance [24, 49, 88] and hence, it was of interest to see if the optical response could be controlled by the photoisomerisation reaction. The appearance and position of the coupled longitudinal plasmon band were monitored for particle clusters linked with *trans* and *cis* azobenzene molecules. In addition, the photoisomerisation of the AZO2-linked structures were studied to see if the particle-to-particle separation in a nanoparticle superstructure could be altered by irradiation of light. The optimal system consisting of two nanoparticles linked with an adjustable linker molecule is illustrated in figure 3.5. In reality, there is a capping ligand layer surrounding the particles and probably more than one molecule bridging the particles into clusters consisting more than two nanoparticles.

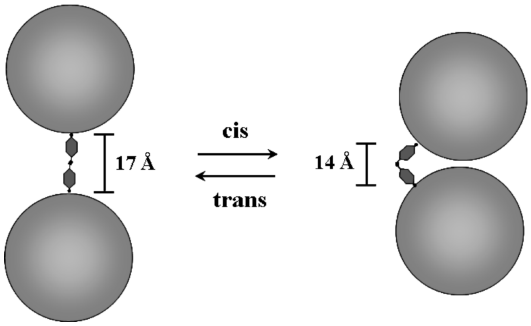

Figure 3.5: Schematic diagram of an idealised system of nanoparticle pair linked with a dithiol molecule. (Reproduced by permission of the PCCP Owner Societies)

A red-shift of the plasmon band due to the appearance of a coupled longitudinal plasmon band was observed resulting from the formation of nanoparticle clusters after cross-linking with the *cis* AZO2. The maximum absorbance wavelength of this secondary plasmon band could be changed by isomerisation of the linker to the *trans* conformer and the spectral changes observed were in rather good agreement with theory and earlier results obtained for gold nanoparticles. [24,88] In the case of nanoparticles linked with the *trans* isomer of azobenzene dithiol, the isomerisation did not influence the appearance of the coupled plasmon band, which implies a rigid structure, where the conformational changes of the linker were restricted.

The surface-to-surface separation of the 3.7 nm AZO2-linked Ag-nanoparticles was approximated from the equilibrium conformation of the molecule obtained with simple chemistry software and assuming that the ligand stands normal to the particle surface. According to this approximation the separation of the surfaces of *cis* AZO2-linked particles would be 6.8 Å and *trans* AZO2-linked particles 17 Å. According to the model presented above these values correspond to 36 and 17 nm plasmon band shifts respectively. The experimentally observed 50 nm shift for the *cis*-linked nanoparticles correspond to a surface-to-surface separation of 4 Å, slightly lower than the expected value. Nevertheless, the model applied in publication III gives a rather good estimation of the observed changes in the optical spectra of the silver nanoparticles functionalised with an azobenzene dithiol. However, the model

does not take into consideration the chemically bound ligand shell surrounding the particles. The effect of the ligands has been studied in literature and is most likely to affect the optical properties of metal nanoparticles. [87]

In publication III, the main goal was to create a switching assembly of silver nanoparticles and azobenzene ligands. The choice of these particular materials was done by their optical properties. According to the experiments performed it was quite obvious that some energy transfer related interaction between the azobenzene chromophore and the plasma surrounding the nanoparticles was obtained. In the case of the dithiol-linked nanoparticle assemblies, changes in the optical spectrum of the nanoparticles were observed after photoisomerisation and could be related to changes in particle-particle separations by a simple theoretical model.

4 Electron transport processes in nano-scale films - characterisation with SECM

4.1 Photoswitching electron transport properties of an azobenzene containing self-assembled monolayer

Molecular wires are an important field of research as potential components in future electrical circuits. Thus, electron transfer via molecular wires plays an important role in nano-scale research. Conventionally single molecule conductance has been studied from the long-range electron transfer through molecular bridges in donor-acceptor systems. [65, 93, 94] Conductance of a molecule has been extracted from charge separation along these donor-acceptor type molecules. [95] More recently, microscopic methods, such as scanning tunneling microscopy (STM), have been successfully employed for measuring charge transfer through single molecules. [96–99] These techniques require molecules with simple terminal groups such as dithiols (see Figure 2.1 b and c) that can be used as contact points. In this chapter, an alternative method for determination of the molecular conductance is presented. In the method considered here, electrical properties of a monolayer consisting of the molecules under interest are studied instead of measuring the properties of a single molecule.

For electrochemists, spontaneous formation of self-assembled monolayers [100, 101] of thiol-terminated molecules on Au(111) surface provides a way for the measurement of molecular conductance. SAMs of thiol molecules have been studied both with conventional electrochemistry [102–104] and with scanning electrochemical microscopy (SECM). [105–108] Previous studies have considered the conductance of both saturated and unsaturated thiolates, but also thiols containing redox centers have been investigated. [106, 109–111] In publication IV SAMs containing azobenzene derivatised thiol (AZO3, figure 4.1 a) were studied. Conductances of SAMs having different fractions of AZO3 and 2-phenylethylthiol (PET, figure 4.1 b) were determined by measuring the rate of electron transfer through the monolayers.

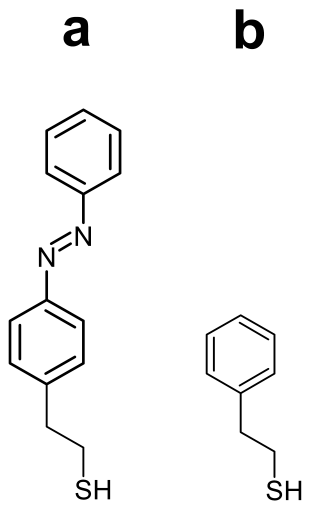

Figure 4.1: Thiols used in the experiments. (a) AZO3, (b) PET.

In publication IV, the barrier properties of mixed monolayers constructed from different amounts of AZO3 and PET were studied by SECM and variable angle ellipsometry. Conformational changes caused by photoisomerisation of the azobenzene groups in the SAMs were also investigated. The thiol monolayers were formed via self-assembly and an Au(111) surface was used as the substrate material to obtain a well defined and smooth surface. Since the self-assembly process from solution to a solid surface is an equilibrium reaction, the final ratio of AZO3 and PET could be determined by their molar ratio in the solution in which the sample was immersed. AZO3/PET concentration ratio was varied so that the AZO3 content of the solution was 100, 80, 60, 40, 20 and 0 %. All the samples were studied both in *trans* and *cis* conformations. Photoisomerisation was carried out by irradiating the sample with 366 nm UV-light and blue light as explained previously in chapter 3.1.

In SECM, an ultramicroelectrode (UME) is immersed in an electrolyte solution containing a redox mediator and moved in close proximity to the surface of interest. In the so called feedback mode, the potential of the electrode is controlled and the current caused by the electrochemical reaction of the redox mediator at the electrode surface is recorded. This mode of SECM is the most commonly used and was

employed in publications IV and V to study the electron transport processes in thin films. Information on the surface properties were extracted from approach curves where the tip current was recorded as a function of the tip-substrate separation.

Different theoretical approaches to solve the diffusion problem of the redox mediator for different electrode sizes and geometries have been made in literature. [112–114] Generally speaking, for each electrode type, the tip current profile depends on the electrochemical activity of the substrate and there are theoretical extremes for totally insulating and conductive substrates between which the measured current curves vary (see figure 4.2). Current response increases when a conductive substrate is approached, because the electrochemical reaction at the substrate recovers the mediator used at the electrode. At an insulating substrate, no such feedback is obtained, since there is no recovery of the reacted mediator at the substrate surface. Hence current actually decreases because the electrode hinders the diffusion of the mediator when the gap to the substrate becomes very small.

In publication IV the rate of the electron transfer between the redox mediator, ferrocenemethanol ($FcMeOH^{0/+}$), and the gold substrate coated with a monolayer of azobenzene molecules was measured. The tip was held at a potential where the reduction of FcMeOH is diffusion limited and the reaction occurring at the substrate surface was assumed to be irreversible. [13, 112, 115] Since diffusion at nanometre-scale is very fast [105] the concentration of the redox mediator at the electrode surface is essentially zero. The mediator was also chosen so that its reaction at the electrode was fast enough for the reaction at the surface to limit the overall reaction rate, which can be extracted from the measured currents.

In figure 4.3, a schematic of the tip geometry is presented. A typical SECM tip is a metal wire embedded in an insulating glass sheath. The very end of the tip is polished carefully so that the cross-section of the tip is circular and the ratio of the total radius r_g and the electrode radius r_e is well defined, typically an integer value, such as 10 or 5. Dimensionless coordinates and parameters used in SECM simulations are explained in terms of the dimensional variables in table 4.1. The general time-dependant diffusion problem at the electrode can be formulated in

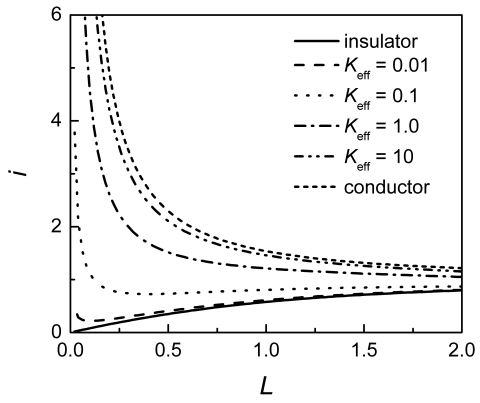

Figure 4.2: Simulated approach curves with K_{eff} values 0.01, 0.1, 1.0 and 10. Solid and dotted lines are the approach curves for insulating and conductive surfaces respectively.

cylindrical coordinates in the following form:

$$\frac{\partial C_i}{\partial T} = \frac{\partial^2 C_i}{\partial Z^2} + \frac{\partial^2 C_i}{\partial R^2} + \frac{1}{R}\frac{\partial C_i}{\partial R} \tag{4.1}$$

where T is the dimensionless time, C_i is the dimensionless concentration of species i, Z is the dimensionless distance normal to the electrode surface and R is the radial dimensionless distance.

There are several ways to obtain the theoretical tip current. In publication IV the approach from Amphlett *et al.* was applied. [114] The tip-substrate dependency of the tip current for insulating substrate, $I_{\text{T}}^{\text{ins}}$, and a conductive substrate, I_{T}^{C}, are found from analytical approximations for the long time limit of the time-dependant diffusion problem and are expressed in equations 4.2 and 4.3 for $RG = 5.1$:

$$I_{\text{T}}^{\text{ins}} = \left[0.48678 + \frac{1.17706}{L} + 0.51241\exp\Big(-\frac{2.07873}{L}\Big)\right]^{-1} \tag{4.2}$$

and

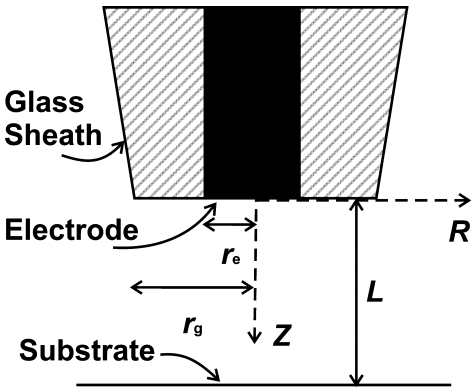

Figure 4.3: Geometry of an SECM tip. Dimensionless coordinates and parameters are explained in table 4.1.

$$I_{\mathrm{T}}^{\mathrm{C}} = 0.72035 + \frac{0.75128}{L} + 0.26651\exp\Big(-\frac{1.62091}{L}\Big) \tag{4.3}$$

where L is the dimensionless tip-substrate separation. For the irreversible substrate kinetics, the tip current within the range $0.1 \leq \mathrm{L} \leq 1$ is given by equation 4.4: [116]

$$I_{\mathrm{T}}^{\mathrm{k}} = \left[\frac{0.78377}{L\Big(1+\frac{1}{\Lambda}\Big)} + \frac{0.68 + 0.3315\exp(-\frac{1.0672}{L})}{1+F(L,\Lambda)}\right] \times \left[\Big(1-\frac{I_{\mathrm{T}}^{\mathrm{ins}}}{I_{\mathrm{T}}^{\mathrm{C}}}\Big) + I_{\mathrm{T}}^{\mathrm{ins}}\right] \tag{4.4}$$

with

$$F(L,\Lambda) = \frac{11 + 7.3\Lambda}{\Lambda(110 - 40L)} \tag{4.5}$$

where Λ is the dimensionless kinetic parameter. From Λ, the dimensionless rate constant for electron transfer, K_{eff}, can be extracted (see table 4.1). Some previous

Table 4.1: Dimensionless variables used in SECM.

Dimensionless variable	
Concentration	$C = \frac{c_{\mathrm{Red}}}{c^{\mathrm{b}}_{\mathrm{Red}}+c^{\mathrm{b}}_{\mathrm{Ox}}} = \frac{c_{\mathrm{Red}}}{c^{\mathrm{b}}}$
Conductivity	$\Sigma = \frac{\sigma k_{\mathrm{B}} T \Delta z}{e^2 r_{\mathrm{e}} D_i c^{\mathrm{b}} N_{\mathrm{A}}}$
Current	$i = \frac{I}{I_{\mathrm{lim}}} = \frac{I}{4nFDc^{\mathrm{b}}r_{\mathrm{e}}}$
Distance normal to the surface	$Z = \frac{z}{r_{\mathrm{e}}}$
Electrochemical potential	$\tilde{\mu} = \frac{\mu-\mu^0}{k_{\mathrm{B}}T}$
Electrode shape factor	$RG = \frac{r_{\mathrm{g}}}{r_{\mathrm{e}}}$
Kinetic parameter	$\Lambda = \frac{k_{\mathrm{eff}} z}{D_i} = K_{\mathrm{eff}} z$
Radial distance	$R = \frac{r}{r_{\mathrm{e}}}$
Standard rate constant	$K^0 = \frac{k^0 r_{\mathrm{e}}}{D_i}$
Time	$T = \frac{tD_i}{r_{\mathrm{e}}^2}$
Tip-substrate separation	$L = \frac{z}{r_{\mathrm{e}}}$

numerical solutions have been published for the diffusion problem in steady-state conditions but they do not consider the so called back diffusion, i.e. diffusion of the redox mediator from behind the plane of the electrode. [112, 115]

Simulated approach curves with varying K_{eff} values are shown in figure 4.2. As K_{eff} is increased from 0.01 to 10 a clear change from negative feedback (current decreasing towards the substrate) to positive feedback (current increasing towards the substrate) is observed. Only values of K_{eff} corresponding to current curves between the extreme negative and positive feedbacks can be used. Consequently, this limits the rate constants that can be measured with this method. However, K_{eff} depends on the rate constant of electron transfer and the diffusion coefficient of the redox mediator (table 4.1) and thus the limits of the accessible values of k_{eff} can be affected by the choice of the redox mediator.

In publication IV, the measured data was normalised by dividing the measured current with the limiting current obtained far from the surface (see table 4.1). The

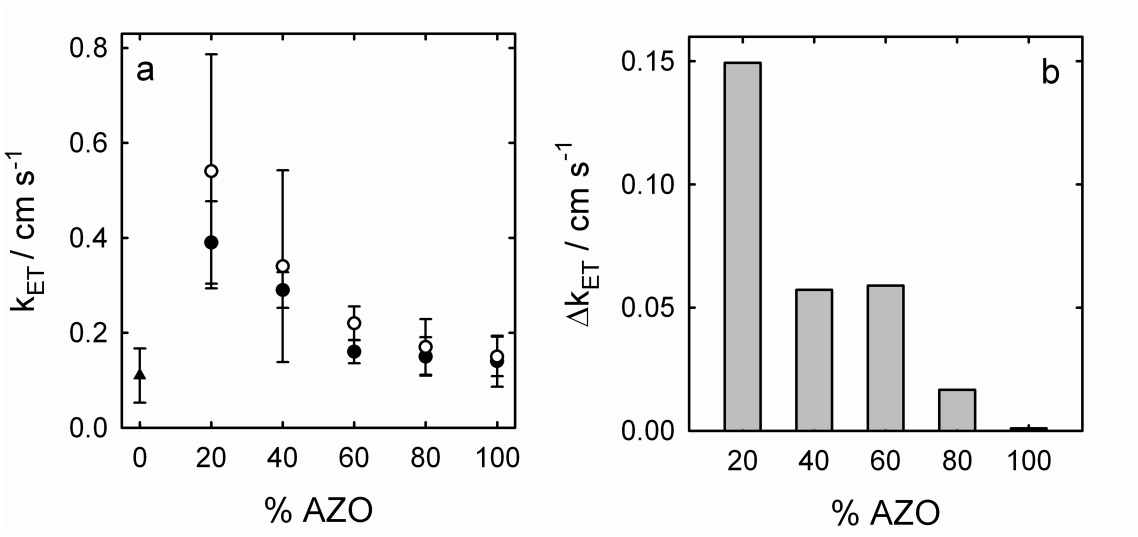

Figure 4.4: (a) Electron transfer rate constants measured for the *trans* SAMs (filled circles), the *cis* SAMs (open circles) and PET SAM (filled triangle). The error bars represent the standard deviation of the apparent rate constants. (b) Differences between the rate constants for *trans* and *cis* SAMs. (Reproduced by permission of the PCCP Owner Societies)

dimensionless current was then fitted to the theoretical approach curve by varying the value of the dimensionless rate constant, K_{eff} from which the effective apparent rate constant k_{eff} [106] for the electron transfer reaction between the mediator and the substrate was determined. Over 15 measurements were performed on each sample to gain a data set representative of the whole sample. The molecular conductance of each monolayer was obtained in terms of the decay constant β, that describes the tunneling rate of electrons through the monolayer.

$$\beta = -\frac{d\ln k_{\text{ET}}}{dr} \tag{4.6}$$

where k_{ET} is the heterogeneous rate constant of electron transfer through the monolayer and r is the thickness of the monolayer.

The measured electron transfer rate constants k_{eff} are presented in figure 4.4 a. Since the monolayers did not include any electrochemically active sites, k_{eff}

corresponds to the rate constant of electron transfer, k_{ET}, across the SAM. [106] The values for k_{ET} obtained in publication IV are significantly larger than those measured for monolayers of alkanethiols [106, 108] because both AZO3 and PET are conjugated and rather highly conductive. [65, 94, 110, 111] A clear decrease of k_{ET} with increasing surface molar fraction of AZO3 is observed implying to the exponential dependence of electron tunneling rate on the layer thickness expressed in equation 4.6, when assuming that the layer thickness scales linearly with the amount of AZO3.

Differences in the heterogeneous rate constants measured for both isomers are shown in figure 4.4 b and a trend between the increasing difference and the SAM composition is observed. This can be explained by considering the steric hindrance in the monolayers. As the relative concentration of the shorter spacer molecules is increased, more pronounced conformational changes of AZO3 are allowed to occur as the free space in the SAM is increased, thus leading to larger differences in the electron transfer rates. The effects of the monolayer composition and the photoisomerisation on the layer thickness were confirmed with ellipsometry. The linear dependence of the thicknesses of the SAM on its composition and the linear dependence of $\ln k_{\text{eff}}$ on the layer thickness are presented in figure 4.5. From the slopes in figure 4.5 b, β values 0.12 Å^{-1} and 0.17 Å^{-1} for the *trans* SAM and the *cis* SAMs were obtained respectively. The lower value of β for trans SAM implies a higher conductance through the monolayer.

There are two possible reasons for the higher conductance of the *trans* SAMs. One is the difference in conductances of the two isomers of azobenzene, which has been predicted and measured by Zhang *et al.* [66, 67] The smaller conductance of *cis* conformer is rationalised in terms of the molecular electronic structure, with the conductance of *cis* azobenzene lower due to the loss of molecular orbital symmetry on isomerisation. [65] Another explanation for the differing barrier properties of the SAMs after conformational changes is the difference in permeation rates of the redox mediator through the monolayers as discussed by Walter *et al.* [117]

As the main result of publication IV, it was demonstrated that photoisomeri-

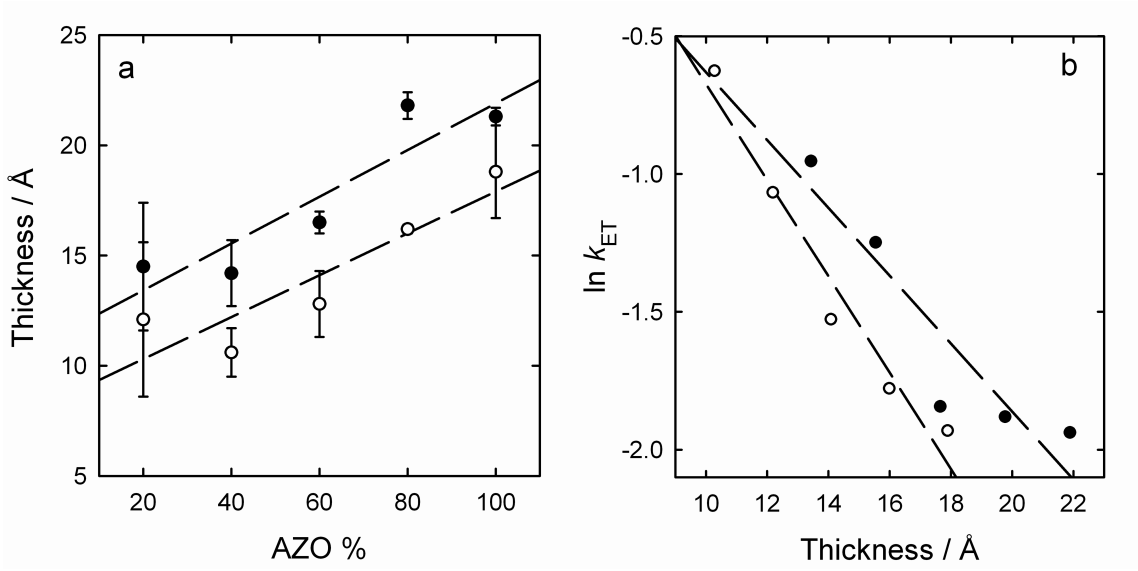

Figure 4.5: (a) The measured thicknesses of the *trans* SAMs (filled circles) and *cis* SAMs (open circles) as a function of the molar fraction of AZO3. The lines are linear fits to the measured data. (b) Dependence of the logarithm of the rate constant for electron transfer on the thickness of the SAM for the *trans* (filled circles) and *cis* (open circles) conformers of AZO3. The thickness scale has been calculated from the linear regression of the results in figure 4.5 a. (Reproduced by permission of the PCCP Owner Societies)

sation leads to measurable changes in the barrier properties of AZO3/PET mixed monolayers. By varying the composition of the SAM, both the effective thickness and the extent of isomerisation could be controlled. It was shown that it is possible to measure the effect of photoisomerisation on the conductance of a SAM containing azobenzene-terminated thiols employing SECM. Combining ellipsometry with SECM allows one to estimate the influence of both the layer thickness and SAM conformation on the barrier properties separately.

4.2 Electrochemical gating in scanning electrochemical microscopy

In publication V the electronic properties of a film formed of monolayer protected clusters (MPCs) were investigated. As MPCs are considered as potential building

blocks for future nanoscale devices, there is considerable interest in their electronic properties. [5,8,101] Monolayer protected clusters are metallic particles coated with an organic shell and they are of particular interest due to their room-temperature quantized charging. [5,8] In practice, it means that MPCs act as multi-valent redox species [8,14,15,118–122] or as diffusing nanoelectrodes. [123] Films of MPCs have been proposed for sensing applications [1,25–30,34,46,124–129] since their electron transport properties are determined by the length and saturation of the protecting ligands and the interparticle separation. [130, 131] In addition the core size and dispersity affect the film conductivity.

Murray and co-workers have demonstrated that for MPC films, electron transport occurs by a bimolecular, electron self-exchange reaction, whose rate is controlled by the tunneling barrier due to the alkanethiolate ligands between the metal cores and the charge state z of the MPC cores. [129] For mixtures of particles with $z = 0$ and $z = 1$, the conductivity was reported to be proportional to the product $[MPC^0][MPC^+]$ and goes through a maximum when these concentrations are equal. [129] This quantised double layer charging is due to Coulomb blockade, which gives rise to periodic metal-insulator transitions at integer values of the average charge state of the particles. [132,133] Thus far, all reported data on Coulomb blockade in MPC films has been obtained using techniques where an electrical connection to the film is a prerequisite to measuring the conductivity. [1,28–30,34,46,125,129] Such films have been prepared either by drop-casting the particles onto a metal electrode for conventional electrochemical experiments or onto an interdigitated array electrode for solid-state conductivity measurements. In the latter case, the $[MPC^0]$ to $[MPC^+]$ ratio was controlled by *ex situ* chemical oxidation of the particles prior to drop-casting the film. [129, 134] The effect of pinholes in the film, counter-ion permeation into thick films and the contact resistance between the film and the electrode are all factors that influence the extracted film conductivity. In the experiments performed in publication V, the film is drop-cast onto an insulating substrate and the measured SECM response is due solely to the film and not any underlying metal electrode. It is shown that the conductance of the film can be measured

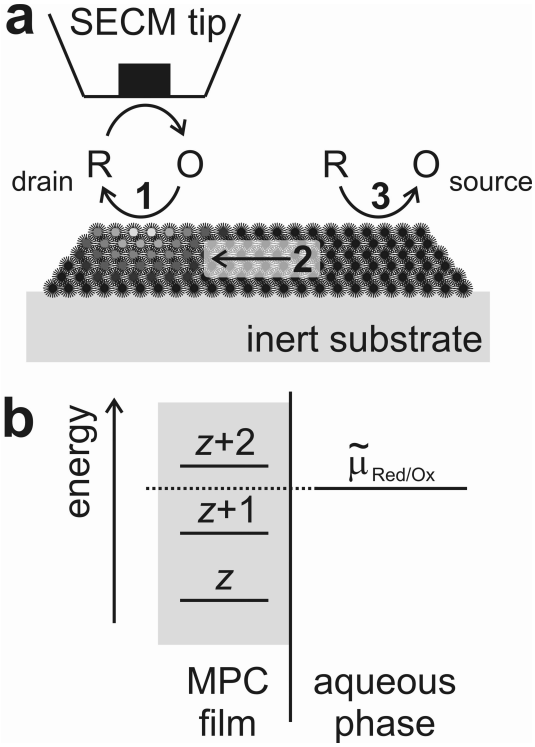

Figure 4.6: (a) Schematic of the experimental setup and the three electron transport processes occurring at the film-electrolyte interface and in the film. (b) Energy level diagram of the experiment. The equilibrium electrochemical potential in the film is set by the nature (standard potential) of the redox couple and the concentration ratio of the oxidised to reduced species. (Reprinted with permission from The American Chemical Society)

as a function of the electrochemical potential without actually connecting it to an external power source.

In publication V, the film conductance was measured by probing the lateral electron transport in a thin MPC film. Although SECM has been utilised in lateral conductivity studies of MPC films and conductive polymer films before, [31, 124, 135–141] some new aspects on these measurements are outlined in publication V. Generally, SECM provides a local, non-invasive probe for the sample conductivity with the added benefit of not having to externally contact the sample. [137, 142] This avoids problems with the contact resistance between the film and the electrical contacts and the resulting ambiguity in the film potential. In a

typical SECM experiment, the film potential is fixed by the equilibrium potential of the redox mediator to a single potential value. [31, 124, 135–141] In publication V however, the interest was on the dependence of the film conductivity on its potential. The electrochemical potential of the thin film of hexanethiolate protected gold nanoparticles was varied through the Nernst equation (equation 4.7) by controlling the ratio of the two forms of the redox mediator in the solution. Also the standard potential of the mediator was varied by using different mediators. The equilibrium potential of the film is given by:

$$E_{\mathrm{eq}} = E^0 + \frac{RT}{F}\ln\left(\frac{c^{\mathrm{b}}_{\mathrm{Ox}}}{c^{\mathrm{b}}_{\mathrm{Red}}}\right) \tag{4.7}$$

where E^0 is the standard redox potential of the redox mediator and $c^{\mathrm{b}}_{\mathrm{Ox}}$ and $c^{\mathrm{b}}_{\mathrm{Red}}$ are the bulk concentrations of the oxidised and reduced forms of the redox species.

In figure 4.6, the principle of the electrochemical gating in the SECM experiment is presented. Since the MPC film is conductive, recovery of the reacted species occurs at the film surface (process 1, drain). In addition, the MPCs are packed quite close to each other in the film so there is also electron transport between them. As a consequence of the feedback from the redox mediator between the electrode and the surface driven by the tip potential, a potential gradient in the film is formed. This gradient causes electron transport in the film (process 2) in the radial direction and leads to a reverse redox reaction between the mediator and the surface (process 3, source). The potential gradient is analogous to the bias difference applied between the source and the drain electrodes in a traditional transport experiment. At the same time, the tuning of the electrochemical potential through the choice and concentration ratio of the redox couple is analogous to gating in the usual three-terminal measurements. Conceptually similar electrochemical gating has been used earlier to gate semiconducting nanoparticle films and carbon nanotubes. [143–145] Setting the equilibrium potential of the film via the electrochemical potential of the solution redox couple is illustrated schematically in figure 4.6 b. The average charge state of the MPCs depend on their potential, and thus can be adjusted by the nature

and concentration ratio of the reduced and oxidised forms of the redox couple.

The studied film was prepared by drop-casting on a glass substrate and consisted of monodisperse hexanethiolate protected Au MPCs having diameter of 1.6 nm. [15,120] The SECM experiments were conducted using the feedback mode, discussed earlier in section 4.1. Families of approach curves were measured by keeping the ratio of the bulk concentrations of oxidised and reduced forms of the redox couple, C^{b} ($= c^{\mathrm{b}}_{\mathrm{Red}}/c^{\mathrm{b}}$), constant and varying the total concentration of the solution, c^{b}. Two redox couples, ferrocene methanol ($\mathrm{FcMeOH}^{0/+}$, $E^0 = 0.21$ V vs. Ag/AgCl) and ferrocene trimethyammonium ($\mathrm{FcTMA}^{+/2+}$, $E^0 = 0.42$ V vs. Ag/AgCl) were used as the aqueous redox mediators. As oxidised forms of the redox couples are not readily available commercially, they were prepared by chemical oxidation of the ferrocene derivatives with $Na_2S_2O_8$. [146] Substrate potential was taken as the equilibrium potential of the mediator in solution determined by $c^{\mathrm{b}}_{\mathrm{Red}}/c^{\mathrm{b}}_{\mathrm{Ox}}$ via the Nernst equation.

Using model that has been described previously, the experimental approach curves could be fitted to yield a quantitative estimate on the electrical conductance of the MPC film. [137] With this model, electron transport in the film is described by equation 4.8, in dimensionless radial coordinates, assuming Ohmic conduction and Gerischer model for electron transfer kinetics [137]

$$\frac{\partial^2\tilde{\mu}}{\partial R^2} + \frac{1}{R}\frac{\partial\tilde{\mu}}{\partial R} - \frac{K^0}{\Sigma}\big((1-C)e^{\tilde{\mu}/2} - Ce^{-\tilde{\mu}/2}\big) = 0 \tag{4.8}$$

$\tilde{\mu}$ is the dimensionless electrochemical potential of the electrons in the film, K^0 is the dimensionless standard rate constant of the electron transfer reaction between the solution redox couple and the nanoparticle film, C the dimensionless concentration of the reduced form of the solution redox couple, and Σ is the dimensionless conductivity in the film.

Outside the tip-substrate gap, the electrochemical potential of the electrons in the MPC film reaches an equilibrium value, μ_{eq}, which is determined by the concentration ratio of the oxidised and reduced forms of the redox couple. Using

this model, families of simulated approach curves were generated using a commercially available finite element simulation package (Comsol Multiphysics, Comsol Ab, Sweden) for each value of μ_{eq} over a wide range of Σ values. As described in the previous publications, [136, 137] the so-called back diffusion was included in the model. Experimental curves were then compared with simulated curves and the corresponding best fit was used to extract Σ. Film conductance was then obtained from the slope of the plot of Σ versus the reciprocal total mediator concentration. With ferrocene derivatives used in this study no kinetic limitations are observed and consequently, all the simulations were carried out with a high value of K^0 (= 10) to give numerically undistinguishable results from $K^0 = \infty$.

In order to validate the proposed method to control the applied potential, approach curves were recorded over a range of total concentration of the redox mediator c^{b} with C^{b} (see table 4.1) fixed to value 0.45 while either reducing (figure 4.7 a) or oxidising (figure 4.7 b) the solution redox mediator at the SECM tip. The observed feedback response in figure 4.7 is a combination of the diffusion flux in the solution and the flux due to electron transport in the film. As the diffusion flux is directly proportional to the total concentration of the redox mediator in solution, the concentration has to be reduced sufficiently to observe electron transport. At high redox couple concentrations, negative feedback due to hindered diffusion to the SECM tip is observed. As the concentration is reduced, the relative contribution of mediator regeneration due to electron transport in the film increases and deviation from purely negative feedback will be observed. This effect is captured by the dimensionless conductivity, Σ. The fitting results are shown in the insets of figure 4.7, where the extracted values of the dimensionless conductivity are plotted as a function of the inverse of the total concentration c^{b} of the solution redox mediator. As expected, these plots are linear. Moreover, as the slope is proportional to the conductance of the film, we measure the same value irrespective whether oxidation or reduction is taking place at the tip.

The actual measurements of the film conductivity as a function of the film equilibrium potential were carried out by varying the concentrations of the oxidised and

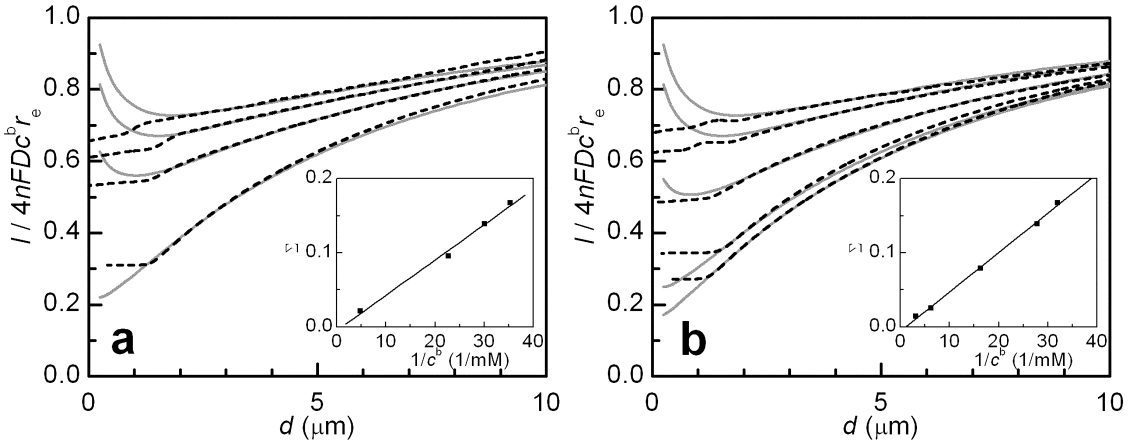

Figure 4.7: Experimental SECM approach curves (dotted lines) along with the fits to simulations (solid grey lines) for the same ratio of the reduced to oxidised forms of the solution redox mediator ($C^{\mathrm{b}} = 0.45$) at different total concentrations c^{b} and tip potentials corresponding to either reduction (a) or oxidation (b) at the SECM tip. Insets: Linear regression of the dimensionless conductivity Σ as function of $1/c^{\mathrm{b}}$. The resulting conductance $\sigma\Delta z$ is $1.58 \times 10^{-10}\ \Omega^{-1}$ for the reduction reaction and $1.55 \times 10^{-10}\ \Omega^{-1}$ for the oxidation of the mediator. (Reprinted with permission from The American Chemical Society)

reduced forms of the solution redox couple and by using two different redox couples with differing standard potentials. With the chosen mediators, the substrate potential could be varied between 137 mV and 460 mV vs. Ag/AgCl. The experimental protocol was repeated for a range of concentration ratios of both redox couples and the dimensionless conductivity was extracted from the slope of the corresponding plots of Σ versus the reciprocal mediator concentration. The conductance values obtained are plotted versus film potential in figure 4.8. Conductance has two maxima with an overall variation of greater than a factor of two within the studied range of electrochemical potentials. A simple model, discussed in publication V, was used to describe the shape of the conductance. A fit to this model for a sum of two charge states is shown by the dashed grey line in figure 4.8. Since the film was formed by drop-casting, its thickness was not precisely controlled and thus variation in the absolute value of conductance and the positions of the charging peaks were observed for different samples. The observation of maxima is in qualitative agreement with

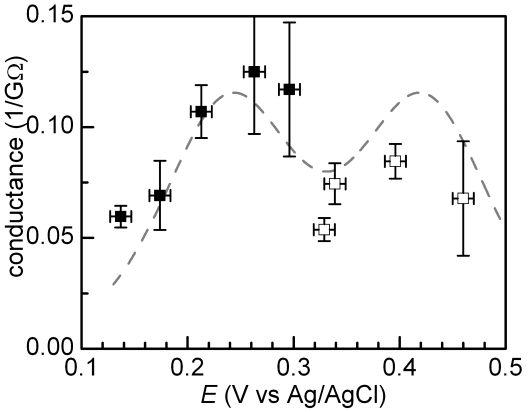

Figure 4.8: Conductance $\sigma\Delta z$ extracted from the fits to the SECM approach curves as a function of the equilibrium electrochemical potential of the MPC film. Redox couple was FcMeOH (filled squares) or FcTMA (open squares). The error bars correspond to the error in the slope of Σ vs. $1/c^{\mathrm{b}}$ as estimated by linear regression analysis. Dashed grey line is a fit to a simple model describing the conductance. (Reprinted with permission from The American Chemical Society)

the reported dependence of film conductance on the degree of mixed valency for nominally identical MPCs. [129, 134] Separation of the maxima in the conductance gives the charging energy of the MPCs in the film (185 meV), which is lower than the value measured for MPCs dispersed in an organic solvent (260 meV). [120] This difference can be attributed to the different dielectric environment of the particles in the film or solution. [147]

As a summary of publication V, it can be stated that SECM can be used to quantitatively measure the potential dependence of electron transport in nanoparticle assemblies without requiring an external electrical connection to the assembly. By using this type of electrochemical gating, issues with the resistance between the film and the electrical contacts could be avoided. It was demonstrated that the conductance of MPC films is strongly dependant on the film electrochemical potential due to room-temperature single-electron charging of the individual MPCs.

5 Conclusions

The main objective of this doctoral thesis was to study different types of self-assembled nanoparticle superstructures and the collective properties of the nanoparticles embedded in them. The thesis was divided into three parts, where the first one considered formation of colloidal nanoparticle superstructures. In publication I, formation of stable clusters of nanoparticles was obtained by chemically bonding silver nanoparticles together with hexanedithiol. The evolution of aggregate size could be readily monitored by dynamic light scattering. After an initial growth period of about 60 minutes, stable aggregates were reproducibly obtained if the reaction was allowed to be under diffusion control. Kinetic information about the thiol exchange reaction could be obtained with a simple model. In summary, it was demonstrated that dynamic light scattering can be applied to study the kinetics of place-exchange reactions on nanoparticle surfaces.

In publication II, the stability of basic aqueous solutions of MUA-capped gold nanoparticles were studied by varying the counter-ions of the hydroxides used to deprotonate the ligand shells of the nanoparticles. A significant difference in the colloid stability was noted with quaternary ammonium ions in comparison to sodium, as these ions did not induce particle coagulation even at very high concentrations. It appeared that the choice of the electrolyte should be carefully considered when using this type of nanoparticles in aqueous environments. An easy modification of the system gave a greatly enhanced stability and even allowed surface reactions that would not proceed otherwise. The colloid stability and the factors affecting it should be taken into account especially in biological applications and in situations where one would rather have a single nanoparticle interaction instead of clusters of electrostatically bound nanoparticles.

The second part of the thesis consisted of a study on nanoparticles functionalised with photoresponsive azobenzene molecules. The optical spectrum of silver nanoparticles linked with azobenzene derivatised dithiol could be controlled by changing the interparticle distance by photoisomerisation of the linker between the

trans and *cis* states. From the results presented in publication III, it could be concluded that photoisomerisation of the photoreactive linker resulted in measurable changes in the coupling of the particles plasmon resonances and that there was interaction between the nanoparticles and the chromophores bound to their surfaces.

The thesis' final part consisted of two studies on applying scanning electrochemical microscopy on studying electron transport processes in thin films. Characterisation of a series of photoresponsive self-assembled monolayers, consisting of azobenzene molecules and aromatic thiolates is presented in publication IV. Isomerisation state of the azobenzene group was shown to affect the conductance across the SAMs. The effect of isomerisation and chemical composition on the thickness of the SAMs was analysed by ellipsometry. It was concluded that both the conformation dependant molecular conductance of the azobenzene molecules and the interaction between the SAM and the redox couple employed affected the conductance of the SAMs.

A study on lateral conductivity of a gold nanocrystal film (publication V) completes this thesis. The effect of the room-temperature quantised charging of the nanoparticles on the film conductivity was observed by measuring the conductivity in several different film potentials. Control on the film potential was achieved from the electrochemical potential of the solution redox couple, which determines the equilibrium potential of the film via the Nernst equation. The advantage of this method was that there was no need for electrical contacts to the film, which usually bring additional resistance to the measured conductivity and thus complicate the analysis of film conductivity.

As a whole, this thesis presents a path from the origin of self-assembly of individual nanoparticles to the collective properties of the formed assemblies. Different approaches towards the use of nanoparticles as building blocks of superstructures were performed. The author hopes that this physicochemical approach, including versatile characterisation and simple models, would give a picture of the inspiration that the author had from the self-assembling functional nanostructures.

References

[1] L. Wang, X. Shi, N. N. Kariuki, M. Schadt, G. R. Wang, Q. Rendeng, J. Choi, J. Luo, S. Lu, and C.-J. Zhong, *Journal of the American Chemical Society*, 2007, **129**(7), 2161–2170.

[2] S. K. Ghosh and T. Pal, *Chemical Reviews (Washington, DC, United States)*, 2007, **107**, 4797–4862.

[3] S. Lee, Z. Guan, H. Xu, and M. Moskovits, *Journal of Physical Chemistry C*, 2007, **111**(49), 17985–17988.

[4] Y. Xiao, F. Patolsky, E. Katz, J. F. Hainfeld, and I. Willner, *Science (Washington, DC, United States)*, 2003, **299**, 1877–1881.

[5] M.-C. Daniel and D. Astruc, *Chemical Reviews (Washington, DC, United States)*, 2004, **104**(1), 293–346.

[6] P. Buffat and J. P. Borel, *Physical Review A: Atomic, Molecular, and Optical Physics*, 1976, **13**, 2287–98.

[7] U. Kreibig and M. Vollmer, *Optical Properties of Metal Clusters. (Springer Series in Materials Science 25)*., 1995.

[8] A. C. Templeton, W. P. Wuelfing, and R. W. Murray, *Accounts of Chemical Research*, 2000, **33**(1), 27–36.

[9] H. Boennemann, G. Braun, G. B. Brijoux, R. Brinkman, A. S. Tilling, K. Seevogel, and K. Siepen, *Journal of Organometallic Chemistry*, 1996, **520**, 143–162.

[10] R. H. Kodama, *Journal of Magnetism and Magnetic Materials*, 1999, **200**, 359–372.

[11] R. D. Vold and M. J. Vold, *Colloid and Interface Chemistry.*, 1983.

[12] M. Stewart, C. Anderton, L. Thompson, J. Maria, S. Gray, J. Rogers, and R. Nuzzo, *Chemical Reviews*, 2008.

[13] A. J. Bard, M. V. Mirkin, and Editors., *Scanning Electrochemical Microscopy.*, Marcel Dekker, Inc., 2001.

[14] D. T. Miles and R. W. Murray, *Analytical Chemistry*, 2003, **75**(6), 1251–1257.

[15] J. F. Hicks, D. T. Miles, and R. W. Murray, *Journal of the American Chemical Society*, 2002, **124**(44), 13322–13328.

[16] C. R. Mayer, S. Neveu, and V. Cabuil, *Advanced Materials (Weinheim, Germany)*, 2002, **14**(8), 595–597.

[17] J. P. Novak and D. L. Feldheim, *Journal of the American Chemical Society*, 2000, **122**(16), 3979–3980.

[18] D. I. Gittins, D. Bethell, D. J. Schiffrin, and R. J. Nichols, *Nature (London)*, 2000, **408**(6808), 67–69.

[19] W. Haiss, R. J. Nichols, S. J. Higgins, D. Bethell, H. Hoebenreich, and D. J. Schiffrin, *Faraday discussions*, 2003, **125**, 179–194.

[20] M. Brust, M. Walker, D. Bethell, D. J. Schiffrin, and R. Whyman, *Journal of the Chemical Society, Chemical Communications*, 1994, (7), 801–802.

[21] M. Brust, D. Bethell, C. J. Kiely, and D. J. Schiffrin, *Langmuir*, 1998, **14**(19), 5425–5429.

[22] S. Fullam, S. N. Rao, and D. Fitzmaurice, *Journal of Physical Chemistry B*, 2000, **104**(26), 6164–6173.

[23] D. Ryan, S. N. Rao, H. Rensmo, D. Fitzmaurice, J. A. Preece, S. Wenger, J. F. Stoddart, and N. Zaccheroni, *Journal of the American Chemical Society*, 2000, **122**(26), 6252–6257.

[24] I. E. Sendroiu, S. F. L. Mertens, and D. J. Schiffrin, *Physical Chemistry Chemical Physics*, 2006, **8**(12), 1430–1436.

[25] A. C. Templeton, F. P. Zamborini, W. P. Wuelfing, and R. W. Murray, *Langmuir*, 2000, **16**(16), 6682–6688.

[26] F. P. Zamborini, J. F. Hicks, and R. W. Murray, *Journal of the American Chemical Society*, 2000, **122**(18), 4514–4515.

[27] F. P. Zamborini, M. C. Leopold, J. F. Hicks, P. J. Kulesza, M. A. Malik, and R. W. Murray, *Journal of the American Chemical Society*, 2002, **124**(30), 8958–8964.

[28] J. F. Hicks, F. P. Zamborini, A. J. Osisek, and R. W. Murray, *Journal of the American Chemical Society*, 2001, **123**(29), 7048–7053.

[29] M. C. Leopold, R. L. Donkers, D. Georganopoulou, M. Fisher, F. P. Zamborini, and R. W. Murray, *Faraday Discuss*, 2004, **125**, 63–76; discussion 99–116.

[30] F. P. Zamborini, L. E. Smart, M. C. Leopold, and R. W. Murray, *Analytica Chimica Acta*, 2003, **496**(1-2), 3–16.

[31] V. Ruiz, P. Liljeroth, B. M. Quinn, and K. Kontturi, *Nano Letters*, 2003, **3**(10), 1459–1462.

[32] I. Hussain, Z. Wang, A. I. Cooper, and M. Brust, *Langmuir*, 2006, **22**(7), 2938–2941.

[33] D. Bethell, M. Brust, D. J. Schiffrin, and C. Kiely, *Journal of Electroanalytical Chemistry*, 1996, **409**(1-2), 137–143.

[34] J. L. Brennan, M. R. Branham, J. F. Hicks, A. J. Osisek, R. L. Donkers, D. G. Georganopoulou, and R. W. Murray, *Analytical Chemistry*, 2004, **76**(19), 5611–5619.

[35] W. P. McConnell, J. P. Novak, L. C. B. III, R. R. Fuierer, R. C. Tenent, and D. L. Feldheim, *Journal of Physical Chemistry B*, 2000, **104**(38), 8925–8930.

[36] G. U. Kulkarni, P. J. Thomas, and C. N. R. Rao, *Pure and Applied Chemistry*, 2002, **74**(9), 1581–1591.

[37] V. Torma, O. Vidoni, U. Simon, and G. Schmid, *European Journal of Inorganic Chemistry*, 2003, (6), 1121–1127.

[38] Z. Zhong, S. Patskovskyy, P. Bouvrette, J. H. T. Luong, and A. Gedanken, *Journal of Physical Chemistry B*, 2004, **108**(13), 4046–4052.

[39] D. S. Sidhaye, S. Kashyap, M. Sastry, S. Hotha, and B. L. V. Prasad, *Langmuir*, 2005, **21**(17), 7979–7984.

[40] R. Mikami, M. Taguchi, K. Yamada, K. Suzuki, O. Sato, and Y. Einaga, *Angewandte Chemie, International Edition*, 2004, **43**(45), 6135–6139.

[41] M. Alvaro, M. Benitez, D. Das, H. Garcia, and E. Peris, *Chemistry of Materials*, 2005, **17**(20), 4958–4964.

[42] Y. Einaga, *Bulletin of the Chemical Society of Japan*, 2006, **79**(3), 361–372.

[43] F. Callari, S. Petralia, and S. Sortino, *Chemical Communications (Cambridge, United Kingdom)*, 2006, (9), 1009–1011.

[44] C. Guarise, L. Pasquato, and P. Scrimin, *Langmuir*, 2005, **21**(12), 5537–5541.

[45] Y. Tan, Y. Li, and D. Zhu, *Langmuir*, 2002, **18**(8), 3392–3395.

[46] N. Krasteva, Y. Fogel, R. E. Bauer, K. Muellen, Y. Joseph, N. Matsuzawa, A. Yasuda, and T. Vossmeyer, *Advanced Functional Materials*, 2007, **17**(6), 881–888.

[47] L. D'Souza, A. Suchopar, and R. M. Richards, *Journal of colloid and interface science*, 2004, **279**(2), 458–463.

[48] R. Pecora, *Journal of Nanoparticle Research*, 2000, **2**(2), 123–131.

[49] S. Y. Park, J.-S. Lee, D. Georganopoulou, C. A. Mirkin, and G. C. Schatz, *Journal of Physical Chemistry B*, 2006, **110**(25), 12673–12681.

[50] A. Charrier, N. Candoni, and F. Thibaudau, *Journal of Physical Chemistry B*, 2006, **110**(26), 12896–12900.

[51] J. Liu and Y. Lu, *Organic & Biomolecular Chemistry*, 2006, **4**(18), 3435–3441.

[52] W. Bo, W. Miao, Z. Hao, S. N. S, T. Weijun, G. Changyou, W. Yanguang, G. Michael, W. Dayang, and M. Helmuth, *Phys Chem Chem Phys*, 2007, **9**, 6313–8.

[53] C. L. Schofield, A. H. Haines, R. A. Field, and D. A. Russell, *Langmuir*, 2006, **22**(15), 6707–6711.

[54] P. Pang, J. Guo, S. Wu, and Q. Cai, *Sensors and Actuators, B: Chemical*, 2006, **B114**(2), 799–803.

[55] J. Wang, A.-N. Kawde, A. Erdem, and M. Salazar, *Analyst (Cambridge, United Kingdom)*, 2001, **126**, 2020–2024.

[56] J.-M. Nam, C. S. Thaxton, and C. A. Mirkin, *Science (Washington, DC, United States)*, 2003, **301**, 1884–1886.

[57] C.-H. Su, P.-L. Wu, and C.-S. Yeh, *Bulletin of the Chemical Society of Japan*, 2004, **77**(1), 189–193.

[58] G. Wang and W. Sun, *The journal of physical chemistry.B, Condensed matter, materials, surfaces, interfaces & biophysical*, 2006, **110**(42), 20901–20905.

[59] R. E. White, J. O. Bockris, B. E. Conway, E. Yeager, and Editors, *Comprehensive Treatise of Electrochemistry, Vol. 1: Double layer.*, 1984.

[60] A. B. Glendinning and W. B. Russel, *Journal of colloid and interface science*, 1983, **93**(1), 95–104.

[61] J. D. Love, *Journal of the Chemical Society, Faraday Transactions 2: Molecular and Chemical Physics*, 1977, **73**(5), 669–688.

[62] T. Kim, K. Lee, M.-S. Gong, and S.-W. Joo, *Langmuir*, 2005, **21**, 9524–9528.

[63] P. Warszynski and Z. Adamczyk, *Journal of Colloid and Interface Science*, 1997, **187**, 283–295.

[64] W. R. Glomm, *Journal of Dispersion Science and Technology*, 2005, **26**(3), 389–414.

[65] M. N. Paddon-Row, *Accounts of Chemical Research*, 1994, **27**(1), 18–25.

[66] C. Zhang, Y. He, H.-P. Cheng, Y. Xue, M. A. Ratner, X. G. Zhang, and P. Krstic, *Physical Review B: Condensed Matter and Materials Physics*, 2006, **73**(12), 125445/1–125445/5.

[67] C. Zhang, M. H. Du, H. P. Cheng, X. G. Zhang, A. E. Roitberg, and J. L. Krause, *Physical Review Letters*, 2004, **92**(15), 158301/1–158301/4.

[68] W. Haiss, H. V. Zalinge, S. J. Higgins, D. Bethell, H. Hoebenreich, D. J. Schiffrin, and R. J. Nichols, *Journal of the American Chemical Society*, 2003, **125**(50), 15294–15295.

[69] Y. Tanaka, A. Inagaki, and M. Akita, *Chemical Communications (Cambridge, United Kingdom)*, 2007, (11), 1169–1171.

[70] H. Qian and J.-Q. Lu, *Physics Letters A*, 2007, **371**, 465–468.

[71] Y. Y. Liang, F. Jiang, Y. X. Zhou, H. Chen, R. Note, H. Mizuseki, and Y. Kawazoe, *Journal of Chemical Physics*, 2007, **127**, 084107/1–084107/6.

[72] T. Hugel, N. B. Holland, A. Cattani, L. Moroder, M. Seitz, and H. E. Gaub, *Science*, 2002, **296**(5570), 1103–1106.

[73] G. Zimmerman, L.-Y. Chow, and U.-J. Paik, *Journal of the American Chemical Society*, 1958, **80**, 3528–3531.

[74] T. Schultz, J. Quenneville, B. Levine, A. Toniolo, T. J. Martinez, S. Lochbrunner, M. Schmitt, J. P. Shaffer, M. Z. Zgierski, and A. Stolow, *Journal of the American Chemical Society*, 2003, **125**(27), 8098–8099.

[75] S. D. Evans, S. R. Johnson, H. Ringsdorf, L. M. Williams, and H. Wolf, *Langmuir*, 1998, **14**(22), 6436–6440.

[76] M. Irie and W. Schnabel, *Macromolecules*, 1981, **14**, 1246–9.

[77] M. Kamenjicki, I. K. Lednev, and S. A. Asher, *Journal of Physical Chemistry B*, 2004, **108**, 12637–12639.

[78] A. Archut, F. Vogtle, L. De Cola, G. C. Azzellini, V. Balzani, P. S. Ramanujam, and R. H. Berg, *Chemistry–A European Journal*, 1998, **4**, 699–706.

[79] B. V. Shankar and A. Patnaik, *Langmuir*, 2006, **22**, 4758–4765.

[80] G. Mie, *Annalen der Physik (Weinheim, Germany)*, 1908, **25**, 377–445.

[81] R. Gans, *Annalen der Physik (Weinheim, Germany)*, 1912, **37**, 881–900.

[82] C. F. Bohren and D. R. Huffman, *Absorption and Scattering of Light by Small Particles.*, 1983.

[83] M. L. Theye, *Physical Review B: Solid State*, 1970, **[3]2**(8), 3060–3078.

[84] P. Mulvaney, *Langmuir*, 1996, **12**(3), 788–800.

[85] S. Link and M. A. El-Sayed, *International Reviews in Physical Chemistry*, 2000, **19**, 409–453.

[86] G. M.-O. L. M. L.-M. Carlos Pecharroman, Jorge Perez-Juste and P. Mulvaney, *Phys. Rev. B*, 2008, **77**(3), 035418.

[87] T. Linnert, P. Mulvaney, and A. Henglein, *Journal of Physical Chemistry*, 1993, **97**, 679–82.

[88] W. Rechberger, A. Hohenau, A. Leitner, J. R. Krenn, B. Lamprecht, and F. R. Aussenegg, *Optics Communications*, 2003, **220**(1-3), 137–141.

[89] K. H. Su, Q. H. Wei, X. Zhang, J. J. Mock, D. R. Smith, and S. Schultz, *Nano Letters*, 2003, **3**(8), 1087–1090.

[90] P. B. Johnson and R. W. Christy, *Physical Review B: Solid State*, 1972, **6**(12), 4370–4379.

[91] U. Kreibig, *Zeitschrift fuer Physik*, 1970, **234**, 307–18.

[92] M. Quinten, *Zeitschrift fuer Physik B: Condensed Matter*, 1996, **101**(2), 211–217.

[93] S. D. Wettig, C.-Z. Li, Y.-T. Long, H.-B. Kraatz, and J. S. Lee, *Analytical Sciences*, 2003, **19**(1), 23–26.

[94] A. Helms, D. Heiler, and G. McLendon, *Journal of the American Chemical Society*, 1992, **114**(15), 6227–6238.

[95] M. D. Newton, *Chemical Reviews (Washington, DC, United States)*, 1991, **91**(5), 767–792.

[96] W. Haiss, H. van Zalinge, D. Bethell, J. Ulstrup, D. J. Schiffrin, and R. J. Nichols, *Faraday discussions*, 2006, **131**, 253–264.

[97] W. Haiss, R. J. Nichols, H. van Zalinge, S. J. Higgins, D. Bethell, and D. J. Schiffrin, *Physical Chemistry Chemical Physics*, 2004, **6**(17), 4330–4337.

[98] S. Wakamatsu, S. Fujii, U. Akiba, and M. Fujihira, *Ultramicroscopy*, 2003, **97**(1-4), 19–26.

[99] D. J. Wold, R. Haag, M. A. Rampi, and C. D. Frisbie, *Journal of Physical Chemistry B*, 2002, **106**(11), 2813–2816.

[100] A. Ulman, *Chemical Reviews (Washington, D. C.)*, 1996, **96**, 1533–1554.

[101] J. C. Love, L. A. Estroff, J. K. Kriebel, R. G. Nuzzo, and G. M. Whitesides, *Chemical Reviews (Washington, DC, United States)*, 2005, **105**(4), 1103–1169.

[102] N. Krings, H. H. Strehblow, J. Kohnert, and H. D. Martin, *Electrochimica Acta*, 2003, **49**(1), 167–174.

[103] M. D. Porter, T. B. Bright, D. L. Allara, and C. E. D. Chidsey, *Journal of the American Chemical Society*, 1987, **109**(12), 3559–3568.

[104] J. Xu, H. Li, and Y. Zhang, *Journal of Physical Chemistry*, 1993, **97**(44), 11497–11500.

[105] A. J. Bard and L. R. Faulkner, *Electrochemical Methods: fundamentals and applications.*, Vol. 7, 2001.

[106] B. Liu, A. J. Bard, M. V. Mirkin, and S. E. Creager, *Journal of the American Chemical Society*, 2004, **126**(5), 1485–1492.

[107] C. Cannes, F. Kanoufi, and A. J. Bard, *Journal of Electroanalytical Chemistry*, 2003, **547**(1), 83–91.

[108] H. Yamada, M. Ogata, and T. Koike, *Langmuir*, 2006, **22**(18), 7923–7927.

[109] K. Weber, L. Hockett, and S. Creager, *Journal of Physical Chemistry B*, 1997, **101**(41), 8286–8291.

[110] S. Creager, C. J. Yu, C. Bamdad, S. O'Connor, T. MacLean, E. Lam, Y. Chong, G. T. Olsen, J. Luo, M. Gozin, and J. F. Kayyem, *Journal of the American Chemical Society*, 1999, **121**(5), 1059–1064.

[111] S. B. Sachs, S. P. Dudek, R. P. Hsung, L. R. Sita, J. F. Smalley, M. D. Newton, S. W. Feldberg, and C. E. D. Chidsey, *Journal of the American Chemical Society*, 1997, **119**(43), 10563–10564.

[112] J. Kwak and A. J. Bard, *Analytical Chemistry*, 1989, **61**, 1221–7.

[113] M. V. Mirkin, F. R. F. Fan, and A. J. Bard, *Journal of Electroanalytical Chemistry*, 1992, **328**(1-2), 47–62.

[114] J. L. Amphlett and G. Denuault, *Journal of Physical Chemistry B*, 1998, **102**(49), 9946–9951.

[115] A. J. Bard, M. V. Mirkin, P. R. Unwin, and D. O. Wipf, *Journal of Physical Chemistry*, 1992, **96**, 1861–8.

[116] C. Wei, A. J. Bard, and M. V. Mirkin, *Journal of Physical Chemistry*, 1995, **99**(43), 16033–16042.

[117] D. G. Walter, D. J. Campbell, and C. A. Mirkin, *Journal of Physical Chemistry B*, 1999, **103**, 402–405.

[118] R. R. Peterson and D. E. Cliffel, *Langmuir*, 2006, **22**(25), 10307–10314.

[119] D. G. Georganopoulou, M. V. Mirkin, and R. W. Murray, *Nano Letters*, 2004, **4**(9), 1763–1767.

[120] B. M. Quinn, P. Liljeroth, V. Ruiz, T. Laaksonen, and K. Kontturi, *Journal of the American Chemical Society*, 2003, **125**(22), 6644–6645.

[121] S. Chen, R. W. Murray, and S. W. Feldberg, *Journal of Physical Chemistry B*, 1998, **102**(49), 9898–9907.

[122] S. Chen, R. S. Ingrma, M. J. Hostetler, J. J. Pietron, R. W. Murray, T. G. Schaaff, J. T. Khoury, M. M. Alvarez, and R. L. Whetten, *Science (Washington, D.C.)*, 1998, **280**(5372), 2098–2101.

[123] J. J. Pietron, J. F. Hicks, and R. W. Murray, *Journal of the American Chemical Society*, 1999, **121**(23), 5565–5570.

[124] V. Ruiz, P. G. Nicholson, S. Jollands, P. A. Thomas, J. V. Macpherson, and P. R. Unwin, *Journal of Physical Chemistry B*, 2005, **109**(41), 19335–19344.

[125] M. P. Rowe, W. H. Steinecker, and E. T. Zellers, *Analytical Chemistry*, 2007, **79**(3), 1164–1172.

[126] F. J. Ibanez, U. Gowrishetty, M. M. Crain, K. M. Walsh, and F. P. Zamborini, *Analytical Chemistry*, 2006, **78**(3), 753–761.

[127] W. P. Wuelfing and R. W. Murray, *Journal of Physical Chemistry B*, 2002, **106**(12), 3139–3145.

[128] J. F. Hicks, S.-S. Young, and R. W. Murray, *Langmuir*, 2002, **18**(6), 2288–2294.

[129] W. P. Wuelfing, S. J. Green, J. J. Pietron, D. E. Cliffel, and R. W. Murray, *Journal of the American Chemical Society*, 2000, **122**(46), 11465–11472.

[130] G. Markovich, C. P. Collier, S. E. Henrichs, F. Remacle, R. D. Levine, and J. R. Heath, *Accounts of Chemical Research*, 1999, **32**(5), 415–423.

[131] C. P. Collier, T. Vossmeyer, and J. R. Heath, *Annual Review of Physical Chemistry*, 1998, **49**, 371–404.

[132] R. E. Chandler, A. J. Houtepen, J. Nelson, and D. Vanmaekelbergh, *Physical Review B: Condensed Matter and Materials Physics*, 2007, **75**(8), 085325/1–085325/10.

[133] D. Vanmaekelbergh and P. Liljeroth, *Chemical Society Reviews*, 2005, **34**(4), 299–312.

[134] J.-P. Choi and R. W. Murray, *Journal of the American Chemical Society*, 2006, **128**(32), 10496–10502.

[135] P. G. Nicholson, V. Ruiz, J. V. Macpherson, and P. R. Unwin, *Phys Chem Chem Phys*, 2006, **8**(43), 5096–5105.

[136] P. Liljeroth and B. M. Quinn, *Journal of the American Chemical Society*, 2006, **128**(15), 4922–4923.

[137] P. Liljeroth, D. Vanmaekelbergh, V. Ruiz, K. Kontturi, H. Jiang, E. Kauppinen, and B. M. Quinn, *Journal of the American Chemical Society*, 2004, **126**(22), 7126–7132.

[138] J. Zhang, A. L. Barker, D. Mandler, and P. R. Unwin, *Journal of the American Chemical Society*, 2003, **125**(31), 9312–9313.

[139] D. Mandler and P. R. Unwin, *Journal of Physical Chemistry B*, 2003, **107**(2), 407–410.

[140] P. Liljeroth, B. M. Quinn, V. Ruiz, and K. Kontturi, *Chemical Communications (Cambridge, United Kingdom)*, 2003, (13), 1570–1571.

[141] B. M. Quinn, I. Prieto, S. K. Haram, and A. J. Bard, *Journal of Physical Chemistry B*, 2001, **105**(31), 7474–7476.

[142] A. L. Whitworth, D. Mandler, and P. R. Unwin, *Physical Chemistry Chemical Physics*, 2005, **7**(2), 356–365.

[143] S. B. Cronin, R. Barnett, M. Tinkham, S. G. Chou, O. Rabin, M. S. Dresselhaus, A. K. Swan, M. S. Unlu, and B. B. Goldberg, *Applied Physics Letters*, 2004, **84**(12), 2052–2054.

[144] D. Yu, C. Wang, and P. Guyot-Sionnest, *Science (Washington, DC, United States)*, 2003, **300**(5623), 1277–1280.

[145] A. L. Roest, J. J. Kelly, D. Vanmaekelbergh, and E. A. Meulenkamp, *Physical Review Letters*, 2002, **89**(3), 036801/1–036801/4.

[146] F.-R. F. Fan and A. J. Bard, *Science (Washington, D. C.)*, 1995, **267**, 871–4.

[147] V. Garcia-Morales and S. Mafe, *Journal of Physical Chemistry C*, 2007, **111**(20), 7242–7250.

ISBN 978-951-22-9361-2
ISBN 978-951-22-9362-9 (PDF)
ISSN 1795-2239
ISSN 1795-4584 (PDF)